United Aircraft Research Laboratories

UNITED AIRCRAFT CORPORATION

EAST HARTFORD, CONNECTICUT

D-910092-6

Experimental Refractive Indices and
Theoretical Small-Particle Spectral
Properties of Selected Metals

NASA Contract No. NASw-847

P. J. Marteney

REPORTED BY N. L. Krascella

W. G. Burwell

APPROVED BY F. S. Owen
Chief, Propulsion

DATE September 1965

NO. OF PAGES 62

COPY NO. 23

FOREWORD

An exploratory experimental and theoretical investigation of gaseous nuclear rocket technology is being conducted by the United Aircraft Corporation Research Laboratories under Contract NASw-847 with the joint AEC-NASA Space Nuclear Propulsion Office. The Technical Supervisor of the Contract for NASA is Captain W. A. Yingling (USAF). Results of the investigation conducted during the period between September 15, 1964 and September 15, 1965 are described in the following eleven reports (including the present report) which comprise the required third Interim Summary Technical Report under the Contract:

1. McFarlin, D. J.: Experimental Investigation of the Effect of Peripheral Wall Injection Technique on Turbulence in an Air Vortex Tube. UAC Research Laboratories Report D-910091-5, September 1965. (Unclassified)

2. Johnson, B. V.: Analytical Study of Propellant Flow Requirements for Reducing Heat Transfer to the End Walls of Vortex-Stabilized Gaseous Nuclear Rocket Engines (U). UAC Research Laboratories Report D-910091-6, September 1965. (report classified Confidential)

3. Travers, A.: Experimental Investigation of Peripheral Wall Injection Techniques in a Water Vortex Tube. UAC Research Laboratories Report D-910091-7, September 1965. (Unclassified)

4. Johnson, B. V., and A. Travers: Analytical and Experimental Investigation of Flow Control in a Vortex Tube by End-Wall Suction and Injection (U). UAC Research Laboratories Report D-910091-8, September 1965. (report classified Confidential)

5. Mensing, A. E., and J. S. Kendall: Experimental Investigation of the Effect of Heavy-to-Light-Gas Density Ratio on Two-Component Vortex Tube Containment Characteristics (U). UAC Research Laboratories Report D-910091-9, September 1965. (report classified Confidential)

6. Krascella, N. L.: Theoretical Investigation of the Opacity of Heavy-Atom Gases. UAC Research Laboratories Report D-910092-4, September 1965. (Unclassified)

7. Kesten, A. S., and R. B. Kinney: Theoretical Effect of Changes in Constituent Opacities on Radiant Heat Transfer in a Vortex-Stabilized Gaseous Nuclear Rocket (U). UAC Research Laboratories Report D-910092-5, September 1965. (report classified Confidential)

8. Marteney, P. J., N. L. Krascella, and W. G. Burwell: Experimental Refractive Indices and Theoretical Small-Particle Spectral Properties of Selected Metals. UAC Research Laboratories Report D-910092-6, September 1965. (Unclassified) (present report)

9. Williamson, H. A., H. H. Michels, and S. B. Schneiderman: Theoretical Investigation of the Lowest Five Ionization Potentials of Uranium. UAC Research Laboratories Report D-910099-2, September 1965. (Unclassified)

10. McLafferty, G. H., H. H. Michels, T. S. Latham, and R. Roback: Analytical Study of Hydrogen Turbopump Cycles for Advanced Nuclear Rockets. UAC Research Laboratories Report D-910093-19, September 1965. (Unclassified)

11. McLafferty, G. H.: Analytical Study of the Performance Characteristics of Vortex-Stabilized Gaseous Nuclear Rocket Engines (U). UAC Research Laboratories Report D-910093-20, September 1965. (report classified Confidential)

Report D-910092-6

Experimental Refractive Indices and Theoretical Small-Particle Spectral Properties of Selected Metals

TABLE OF CONTENTS

	Page
SUMMARY	1
RESULTS	2
INTRODUCTION	3
OPTICAL PROPERTIES OF METALS	4
MEASUREMENT OF COMPLEX REFRACTIVE INDEX OF METALS	7
Experimental Apparatus	7
Alignment and Calibration	9
Experimental Procedure	10
Results of Experimental Measurements	11
Discussion	12
THEORETICAL INVESTIGATION OF THE EXTINCTION, ABSORPTION, AND ROSSELAND MEAN OPACITY PARAMETERS OF SOLID PARTICLES	13
Mie Theory	13
Results of Mie Calculations	15
Rosseland Mean Opacity Parameter of Tungsten Particles	16
REFERENCES	18
LIST OF SYMBOLS	21

TABLE OF CONTENTS
(Continued)

Page

APPENDIXES

I - EQUATIONS RELATING THE COMPLEX REFRACTIVE INDEX TO EXPERIMENTAL QUANTITIES 24

II - DATA REDUCTION AND PRECISION IN ELLIPSOMETER MEASUREMENTS 26

TABLES I - II 29

FIGURES 1 - 32 31

Report D-910092-6

Experimental Refractive Indices and Theoretical Small-Particle Spectral Properties of Selected Metals

SUMMARY

13827

An applied research program was conducted to determine the absorption, scattering, and extinction parameters of small spherical metal particles which might be employed as seeding agents to control radiant heat transfer in gaseous nuclear rocket engines. This program consisted of both experimental and theoretical phases. Under the experimental phase of the program, measurements were made using an ellipsometric technique to determine the complex refractive indices of hafnium, molybdenum, nickel, and tungsten in the wavelength range between 0.2 and 0.7 microns. Under the theoretical phase of the program, calculations were made using the Mie theory to determine spectral absorption, scattering, and extinction parameters of small spherical particles made from nine different metals. These calculations were made using values of the complex refractive indices of the four metals investigated in the experimental phase of the program and the complex refractive indices for cobalt, iron, titanium, vanadium, and zirconium determined from the current literature. Calculations were also made of the Rosseland mean opacity parameter of 0.05μ-radius tungsten particles using spectral absorption parameters determined from the Mie theory. Author

RESULTS

1. The variations with wavelength of the real and imaginary parts of the complex refractive index of hafnium, molybdenum, nickel, and tungsten are smooth and continuous between 0.2 and 0.7 microns. In general, these indices increase with increasing wavelength; these increases are typical of metals not exhibiting absorption bands within the wavelength range investigated.

2. The greatest absorption parameter computed using the Mie theory and complex refractive indices measured in the program is that for nickel and is equal to 4.5×10^4 cm^2/gm for a wavelength of 0.42μ and a particle radius of 0.05μ.

3. Measured values of the real and imaginary parts of the complex index of refraction of molybdenum, nickel, and tungsten are somewhat smaller in magnitude than values found in literature references. These differences are regarded as being due to surface treatment of the samples rather than to experimental errors.

4. The complex refractive index of hafnium, for which no reference data are available, was found to vary from $1.58 - 1.30i$ at 0.2μ to $2.47 - 2.67i$ at 0.7μ. In general, refractive indices are within 10 to 20 percent of the corresponding values for tungsten, but differ by greater percentages from those for molybdenum and nickel.

INTRODUCTION

The introduction of particle seeds into gaseous media to control radiant heat transfer is of general interest for all types of rocket engines, and the use of such seeds is probably a necessity for gaseous nuclear rockets in which the absorption of thermal radiation emanating from the gaseous nuclear fuel is the primary mode of energy deposition in the propellant (for example, in the concept of Ref. 1). The use of particle seeds to control radiant heat transfer may also be of interest for solid-core nuclear rockets (Ref. 2). Therefore, it is desirable to obtain information on the absorption, scattering, and extinction characteristics of particles made from a variety of materials over a wide range of conditions.

Two techniques have been employed to obtain information on the absorption and scattering characteristics of particle seeds. The first method involves measurement of the light transmission and scattering which occurs in tests with a light beam incident on a gas or liquid containing a cloud of small particles. Results obtained using this technique are given in Refs. 3 through 8. The second technique consists of the calculation of the absorption and scattering characteristics of spherical particles from the Mie theory (Ref. 9) using experimentally determined values of the complex refractive index of the particle material. Typical results obtained by this second technique are given in Ref. 10. The second technique was adopted for use in the program described in the present report because it deals directly with the optical properties of the materials involved and because it does not encounter the problem of particle agglomeration which has a large effect on results obtained by the first technique.

Although measurements have been made to determine the complex index of refraction of a variety of materials over a range of wavelengths, the calculations of particle absorption and scattering characteristics in Ref. 10 were limited in scope because insufficient information was available on many materials of interest, particularly in the ultraviolet portions of the spectrum. Therefore, the object of the present tests was to supplement available experimental information on the complex index of refraction of various materials and to employ this information in the calculation of the absorption and scattering characteristics of particle seeds which might be used in gaseous nuclear rockets.

OPTICAL PROPERTIES OF METALS

Two of the optical properties associated closely with metals, and largely distinguishing them from other forms of matter, are high refractivity and low transmission of incident electromagnetic radiation. These properties may be described in terms of a complex refractive index, $N = n - ik$, where n is termed the real part and k the imaginary part of the index. The real part of the refractive index, related to refraction, reflection, and scattering, is expressed in terms of Snell's law,

$$n / n' = \sin \phi / \sin \phi' \tag{1}$$

which describes the change in direction of light caused by a change in refractive index. The imaginary part of the refractive index, sometimes called the extinction coefficient, is related to the spectral absorption coefficient α_ω by

$$\alpha_\omega = 4\pi k / \lambda \tag{2}$$

where α_ω is the absorption coefficient in Lambert's law

$$I / I_0 = e^{-\alpha_\omega x} \tag{3}$$

The unique character of the refractive index of metals is illustrated by the approximate values of n and k commonly encountered in different phases and types of materials. For example, the real portion of the refractive index for gases at 273 K and 1 atm typically lies between 1.00004 (helium) and 1.002 (gaseous organic compounds), relative to $n_{vacuo} = 1.0$ (Ref. 11). The imaginary part of the complex refractive index for gases is determined by the optical transitions in the gas at any given wavelength. The approximate magnitude of α_ω for HCl in an absorption band at a wavelength of 0.16μ is 10^{-1} cm^{-1} at a temperature of 1740 K and pressure of 29 atm (Ref. 4), which corresponds to $k = 4 \times 10^{-6}$. Truly transparent gases, such as air in the visible region under ambient conditions, may have complex parts of the refractive index of the order of 10^{-9}. Liquids, in general, exhibit values of n between 1.0 and 2.0 (Ref. 11), and values of k related by the mass density ratio to those of gases. The refractive index of molybdenum, by contrast, has been given as $N = 3.59 - 3.40\,i$ at 0.546μ (Ref. 12); molybdenum is highly refractive and strongly absorbing.

It is usually convenient to measure the two components of the refractive index of fluids in two separate experiments. That is, the change of direction of a light beam, related to n as in Eq. (1), may be measured without reference to the negligible absorption by the fluid, and the extinction coefficient, k, may be obtained directly (using Eq. (2)) from the spectral absorption coefficient utilizing generally convenient path lengths, typically in the millimeter to meter range. However, inspection of Eqs. (2) and (3) and substitution of a typical metallic value of $k = 3.0$ reveals that, at 0.5μ, 50% absorption would be achieved by a metal having a thickness of only 0.01μ. In general, it is more convenient to determine both parts of the complex refractive index of metals simultaneously by reflection methods utilizing evaporated films or bulk material than to attempt to utilize transmission methods and find n and k separately.

Polarized light incident upon a surface can be resolved into perpendicular components. The two components generally suffer unequal phase and amplitude changes on reflection. Two principal experimental methods have been developed to relate these changes to the complex refractive index of a surface. The first procedure (Refs. 13, 14, and 15) involves the measurement of the reflection coefficients of a surface using plane polarized light having a specific plane of polarization, either parallel or perpendicular to the surface. It is necessary to employ two complementary angles of incidence, as, for example, 20 deg and 70 deg. The equations which relate to this method are given in APPENDIX I, Eqs. (I-1) through (I-4). However, a direct solution for the index of refraction from the experimental data is not practical, even with high-speed computers. Instead, it is convenient to compute the reflection coefficients from selected values of n and k and interpolate graphically (Ref. 13). Disadvantages of this method are the errors associated with interpolation, the necessary change in sample orientation and alignment, and the need to measure light intensities.

An alternate means of determining the complex refractive index of a surface is the method of polarizing spectrometry, or ellipsometry (Refs. 16 through 19). In this procedure, elliptically polarized light is directed at the surface so that there are components both parallel and perpendicular to the surface. When the incident beam is properly oriented, the reflected beam is plane polarized. In this method the actual experimental quantities observed are directly related to the phase and amplitude changes of the two components. The pertinent equations are given in APPENDIX I, Eqs. (I-6) through (I-9). As with the first method, recourse to high-speed computers is necessary, but n and k can be computed more readily from observed quantities than in the previous instance, and the errors of interpolation do not occur (Ref. 20). In addition, the two parameters pertinent to the measurements are obtained without regard to light intensity, except that the process involves detection of a minimum in net transmission. This method requires no shift in optical alignment at any time. One disadvantage is the greater number of optical components utilized in the measurements, but this is only significant in

the initial alignment. Because of the overall advantages, the ellipsometric method was employed in the measurements described in this report; data reduction was accomplished by means of a machine program run on the IBM 7094-2 computer (Ref. 20).

MEASUREMENT OF COMPLEX REFRACTIVE INDEX OF METALS

Experimental Apparatus

The ellipsometer may be regarded as a polarizing spectrometer. As such, it possesses features common to most spectrometers. A light source, sample holder and detector are employed, with the addition of the polarizing components. A schematic diagram of the ellipsometer is shown in Fig. 1. This instrument is generally similar to that used in Ref. 17.

The polarizing components included a polarizer and an analyzer (both Nicol prisms) and a compensator. The polarizer and compensator were mounted in series between the source and sample, and the analyzer was mounted between the sample and detector. The function of the polarizer was to provide plane polarized light from the unpolarized monochromator beam. The plane of polarization was referred, as were all azimuthal orientations along the light path, to the plane containing the normal to the sample and the light beam, i.e., to the plane of incidence. The orientation of the plane of polarization (or polarizer axis) was determined by the rotation of a divided circle on which the polarizer was mounted. The first of two experimental parameters, P, was the polarizer orientation. The compensator was used to separate the plane polarized light into perpendicular components and introduce a phase difference, thus producing elliptically polarized light. The compensator consists of a pair of quartz wedges having the optic axes parallel and a flat plate whose optic axis is at 90 deg to the wedges. Light traveling a greater distance with the plane of polarization parallel to the optic axis undergoes a retardation, and the phase difference results. The compensator was always used with the "fast" axis, i.e., the flat plate optic axis, at -45 deg to the plane of incidence, and was adjusted by moving one wedge to produce 90 deg relative retardation between the two light components at each wavelength. For a specific complex refractive index, a particular setting of the polarizer, P, leads to plane polarized light on reflection from the surface. Through rotation of the analyzer until a minimum signal reaches the detector, it is possible to determine the orientation of the plane of polarization of the reflected light. This manipulation yields the second experimental parameter, which is the analyzer setting, A. Other fixed experimental conditions were the wavelength, material, and angle of incidence.

Samples utilized in these investigations were MRC Corporation zone-refined, polycrystalline rods 0.25 in. in diameter and 0.15 to 0.25 in. in length, which were polished with 0.05μ abrasive, chemically cleaned, and cemented into 0.25-in. diameter holes in microscope slides. The slides were mounted on a Charles Supper X-ray goniometer which was attached to the sample table.

In order to use the most efficient optical system at each wavelength, the measurements were performed in three wavelength intervals, and some optical components were unique to each interval. The three wavelength intervals used were 0.35 to 0.7μ (visible), 0.3 to 0.45μ (near UV), and 0.2 to 0.35μ (deep UV).

System Employed in Visible Measurements (0.35 to 0.7μ)

The source for the visible measurements was a 100-watt incandescent tungsten filament microscope illuminator powered by a 6-volt battery supply for stability. The continuous spectrum was dispersed by a Bausch and Lomb monochromator Model 33-86-25, which utilizes a diffraction grating. Wavelength bandpass was of the order of 30 Å, and the grating was operable from 0.35 to 0.8μ in first order. The compensator was a Crystal Optics Babinet-Soleil type, which is useful from the vacuum UV well into the infrared. The polarizers were Crystal Optics Glan-Thompson prisms manufactured from calcite, and transmitted from approximately 0.2μ through the infrared. These components were fixed to a rigid metal bench. The detector was an RCA 1P21 photomultiplier tube mounted in a shielded housing; the output signal was amplified and displayed by a Photovolt photometer. The analyzer and detector were mounted on an arm which pivoted about a vertical axis intersected by the optical axis of the fixed components. The sample was mounted on a table which rotated about the same vertical axis.

System Employed in Near Ultraviolet Measurements (0.3 to 0.45μ)

The source of ultraviolet light was a 1000-watt Hanovia xenon-mercury lamp operated at approximately 35 volts and 25 amperes across a stabilized power supply. This source provides both strong mercury lines and a rich continuum. The desired wavelengths were obtained by means of a Perkin-Elmer Model 99 double-pass monochromator using an 1800-lines/mm diffraction grating. The monochromator was operated with blocking which prevented mixing of light of an undesired wavelength with the desired monochromatic beam.

Two overlapping wavelength ranges of 0.18 to 0.36μ and 0.32 to 0.5μ were available. With the entrance slit width of 0.5 mm employed, wavelength bandpass was approximately 4 Å.

The detector employed for the near UV measurements was an EMI6255-B end-on photomultiplier tube whose output was displayed either on the photometer used in the visible measurements or on a Hewlett-Packard VTVM; the remainder of the system was unchanged from that employed in the visible region measurements.

System Employed in Deep Ultraviolet Measurements (0.2 to 0.35μ)

Measurements between 0.2 and 0.35μ were conducted using additional spectral refinements which were designed to eliminate the undesirable influence of stray light. A 13-cps chopper in the Perkin-Elmer monochromator was operated in conjunction with a tuned amplifier. In this manner, only the desired light signal was sensed by the amplifier system. An RCA 1P28 phototube was utilized; the signal was amplified and displayed on a strip-chart recorder. Significant reduction in stray light was achieved by substitution of a grating having 1200 lines/mm. This permitted operation between 0.2 and 0.45μ in one range and facilitated sample alignment through the use of visible light. With the slit width of 0.5 mm employed, wavelength bandpass was approximately 6 Å.

Alignment and Calibration

Alignment of Optical Components

The optical alignment of the ellipsometer proceeded in several steps, viz., (1) the alignment of the optical axes, (2) fixing of relative orientation of the polarizer, analyzer, and compensator.

Alignment of Optical Axis

The overall optical alignment of the instrument was facilitated by regarding the pivot axis of the detector arm as a reference axis. At the start of the alignment only the tungsten source and Bausch and Lomb monochromator were in position. A Kollmorgan Company illuminated collimator was attached to the detector arm using a parallel spacer plate. A first-surface silvered mirror was positioned at the sample location and aligned using the collimator. The collimator beam and the monochromator beam were then compared by rotating the sample table until the mirror faced the incident beam; adjustment of the monochromator source assembly to yield reflection along the incident axis assured that all components lay in the same optical plane. Insertion of each remaining component was followed by rechecking.

Alignment of Polarizer and Analyzer Mounts

The polarizer and analyzer holders were aligned so that their reference plane of transmission was at 0 deg to the plane of incidence, which is the plane including the optical path and the normal to the sample surface. This was accomplished in two steps (Ref. 17). First, the polarizer and analyzer were adjusted through observation of transmitted light intensity so that, at minimum intensity, $P = A \pm 90$ deg. Then, with an aligned metal surface used for reference, the mounts were adjusted until the minimum transmission fell at $P = 0$ deg and $A = 90$ deg. This procedure is the most critical of the entire alignment, as any residual ellipticity

(net error in zero position of the polarizer or analyzer) affects the results. The final average error in orientation of either the polarizer or analyzer mounts was less than 0.03 deg (2 minutes of arc).

Calibration of the Compensator

The Babinet-Soleil compensator is capable of providing phase difference (retardations) of approximately -3 to +10 waves in the components of light passing through it. In these studies, a phase difference of 90 deg was desired. While the manufacturer provides a table of wedge adjustment per full wave difference, the zero phase displacement setting is not given. Therefore, calibration is required in the vicinity of the wavelength employed. This was effected by observing the 0, -1, and +1 wave displacement settings at selected wavelengths through the spectrum with the compensator oriented at an azimuth of -45 deg. Differences between the observed settings and manufacturer's specifications were negligible. The + 1/4-wave settings were therefore calculated from the observed zero- and full-wave displacement settings.

Calibration of Monochromators

The wavelength calibration of the Bausch and Lomb monochromator is fixed at time of manufacture; the grating and grating rotation assembly are mounted essentially permanently on the top cover of the monochromator. Although the entire cover is replaced to change from UV to visible or IR, the grating carriage need not be disturbed. The calibration was checked, however, by using interference filters to assure that wavelengths indicated did fall within the filter transmission band. This was found to be valid at 0.365, 0.436, and 0.546μ.

The Perkin-Elmer monochromator, on the other hand, is widely adjustable and therefore has no factory calibration. With the grating having 1800 lines/mm, overlapping intervals of approximately 0.18μ are available by step changes in the grating carriage position. The carriage was adjusted so that the intervals 0.18 to 0.36μ and 0.31 to 0.49μ were available. Known mercury lines were taken as wavelength standards to obtain the relation of grating drive setting to wavelength in each of the two carriage positions. The same procedure was followed to calibrate the grating having 1200 lines/mm except that the interval 0.2 to 0.45μ was utilized.

Experimental Procedure

Preliminary adjustments to the system included warmup of electrical systems and the source, orientation of the polarizer and analyzer divided circles at 0 deg (plane of polarization parallel to the plane of incidence) and orienting the compensator fast axis at the required azimuth of -45 deg.

The microscope slide holding the sample was clamped to the goniometer and, with the sample table adjusted to 0 deg, the slide was manipulated so that the incident beam was reflected directly back onto a limiting aperture. Then the sample table was rotated to yield the angle of incidence employed (generally 65 deg), and the detector arm was pivoted to receive the reflected beam. The monochromator and compensator were then adjusted according to the respective calibrations for the wavelength of light being employed.

The polarizer and analyzer divided circles were then rotated in turn until a minimum signal reached the detector. (Approximately four motions of each circle were required to locate the deepest minimum.) The P and A settings were recorded. Representative values of the first settings, P_1 and A_1, were 17.55 deg and 28.23 deg, respectively, for the hafnium sample at 0.55μ. Next the polarizer was rotated to 90 deg and the analyzer was reset to 0 deg. The adjustment process was repeated as above, this time yielding (for hafnium at 0.55μ) P_2 and A_2 values of 108.62 deg and 331.67 deg, respectively. The method of reducing the raw data is summarized in TABLE I. For this specific case, the values of p_1 and p_2 are 17.55 and 18.62 deg, and the values of α_p and α_s are 28.23 and 28.33 deg, respectively. The subscript on "α" refers to the inclination of the ellipse describing the incident beam of light with respect to the plane of incidence. The two values always differ slightly, and it is presumed that all significant error is removed by the averaging of α and α (See APPENDIX II for a discussion of this point). The complex refractive index was computed using the averages of the reduced experimental quantities p_1 and p_2 and α_p and α_s, respectively.

Results of Experimental Measurements

The organization of the figures on which the results of this investigation are plotted is given in TABLE II. Also listed on this table are the figures on which complex refractive indices obtained from the literature (Refs. 12, 14, and 21 through 25) are plotted. The real and imaginary parts of the refractive index determined from measurements performed using hafnium, molybdenum, nickel, and tungsten are shown in Figs. 2 through 5 as functions of wavelength. All data for each metal are shown together with a smooth curve faired through the data.

The experimental results for hafnium are shown in Fig. 2. The complex refractive index exhibits a slow, regular decrease from 0.7 to 0.27μ. Below 0.27μ the complex part becomes smaller in magnitude than the real part. The refractive index at 0.2μ is $N = 1.58 - 1.30i$. No relevant reference data are available for comparison.

The experimental results for molybdenum are displayed in Fig. 3 in the same fashion as for hafnium. Literature data (Ref. 12) are shown in Fig. 3 for wavelengths of 0.436, 0.549, and 0.579μ. The refractive index of molybdenum varies from $N = 3.02 - 2.65i$ at 0.7μ to $1.13 - 2.50i$ at 0.2μ.

The results for nickel are shown in Fig. 4. The real part of the refractive index exhibits a smaller variation with wavelength in nickel than in any other of the materials examined. The refractive index varies from $= 0.91 - 2.89i$ at 0.7μ to $N = 0.41 - 1.51i$ at 0.2μ. Relevant literature data (Ref. 12) are shown in Fig. 4 for wavelengths of 0.436 and 0.58μ.

Tungsten data are shown in Fig. 5. For tungsten, the refractive index varies from $N = 2.50 - 300i$ at 0.7μ to $N = 1.06 - 1.82i$ at 0.2μ. Limited data (Ref. 12) are available for comparison and are shown for 0.57 and 0.58μ on Fig. 5.

Discussion

There are spectral regions of close agreement between existing data and the results of this investigation, particularly for k. For the complex part of the refractive index for molybdenum and tungsten, these measurements and some available literature values differ by only about 10%, although, in the case of tungsten, other sources are in disagreement by approximately 15%. The complex part for nickel differs from previously determined values by about 25%. The real part of the refractive index differs by approximately 40% from the literature values for molybdenum, 50% for nickel, and 25 and 40% for the two sources cited in Ref. 12 for tungsten.

Literature data employed for comparison in Figs. 3 to 5 are all for polished, bulk material (Ref. 12). Alternate forms of surface treatment such as etching, cleaving, surface heating or bombardment, and formation of the surface by evaporation--all tend to yield different results (Refs. 14, 15, 22, and 26); in general, the vacuum-maintained, highly clean surfaces (Refs. 14, 15, and 22) yield the largest refractive indices, and polished samples yield the smallest complex indices. Greater differences can be found between separate measurements on nominally similar surfaces (Ref. 12) than the differences between the results of the present report and literature data. Cleaved surfaces or evaporated films exhibit the highest refractive indices; it is known that polishing of either type of surface, while not affecting the flatness or reflectivity, leads to a reduction in the measured n and k. It has been concluded that polishing such as that employed in the measurements tends to produce, even in crystalline samples, a surface whose properties are more closely amorphous in nature (Ref. 22).

THEORETICAL INVESTIGATION OF THE EXTINCTION, ABSORPTION, AND ROSSELAND MEAN OPACITY PARAMETERS OF SOLID PARTICLES

Mie Theory

Electromagnetic radiation incident upon matter is, in general, partially absorbed and partially scattered. The sum of the absorption and scattering processes is termed extinction. The extinction of radiation by small solid particles surrounded by a continuous matrix (a gas or liquid) may be analyzed theoretically by the solution of Maxwell's electromagnetic equations with appropriate boundary conditions. The solution for the case of plane wave radiation incident upon spherical particles of refractive index N_1 surrounded by a continuous matrix of refractive index N_2 was first formally solved by Mie (Ref. 9). The Mie theory is the basis for the UARL machine computation program employed to estimate the spectral extinction and absorption parameters of small solid particles applicable as seeding agents in the propellant region of a gaseous core nuclear rocket (Ref. 1). Only a summary of the pertinent equations will be presented in this report. A detailed analysis of the machine program is given in Ref. 10.

The fundamental Mie equations for evaluating the spectral properties of small spherical particles are (Refs. 9 and 10):

$$\sigma_e = \frac{2\pi R^2}{\alpha^2} \sum_{m=1}^{\infty} (2m+1)\, \mathrm{Re}\,(a_m + b_m) \tag{4}$$

$$\sigma_s = \frac{2\pi R^2}{\alpha^2} \sum_{m=1}^{\infty} (2m+1)\left(|a_m|^2 + |b_m|^2\right) \tag{5}$$

$$\sigma_a = \sigma_e - \sigma_s \tag{6}$$

where the σ's are the extinction, scattering, and absorption cross-sections per particle; R, the particle radius; a_m and b_m, the Mie coefficients; and α, a dimensionless size parameter. The quantity α is defined by:

$$\alpha = \frac{2\pi R}{\lambda} = 2\pi \times 10^{-4}\, R\omega \tag{7}$$

where λ is the wavelength of the incident radiation and ω the reciprocal of λ or the wave number. The Mie coefficients a_m and b_m are analytically represented by:

$$a_m = -\frac{j_m(\bar{N}\alpha)\left[\alpha\, j_m(\alpha)\right]' - j_m(\alpha)\left[\bar{N}\alpha\, j_m(\bar{N}\alpha)\right]'}{j_m(\bar{N}\alpha)\left[\alpha\, h_m^{(2)}(\alpha)\right]' - h_m^{(2)}(\alpha)\left[\bar{N}\alpha\, j_m(\bar{N}\alpha)\right]'} \tag{8}$$

$$b_m = -\frac{j_m(\alpha)\left[\bar{N}\alpha\, j_m(\bar{N}\alpha)\right]' - \bar{N}^2 j_m(\bar{N}\alpha)\left[\alpha\, j_m(\alpha)\right]'}{h_m^{(2)}(\alpha)\left[\bar{N}\alpha\, j_m(\bar{N}\alpha)\right]' - \bar{N}^2 j_m(\bar{N}\alpha)\left[\alpha\, h_m^{(2)}(\alpha)\right]'} \tag{9}$$

where $\bar{N}$ is the refractive index of the particle N_1, relative to that of the medium N_2.

$$\bar{N} \equiv N_1 / N_2 \tag{10}$$

The quantities $j_m(\ )$ and $h_m^{(2)}(\ )$ are spherical Bessel and Hankel functions while the primes denote differentiation with respect to the argument of the Bessel or Hankel functions.

The equations outlined above permit analysis of the extinction, scattering, and absorption cross-sections for spherical particles as a function of particle radius if the refractive indices of the particle and matrix materials are known as a function of wavelength. In the UARL program (Ref. 10) the refractive index of the matrix material is assumed to be unity, therefore:

$$\bar{N} = N_1 = N = n - ik \tag{11}$$

where n is the real part and k the imaginary part of the refractive index of the particle material.

The cross-sections for extinction, scattering, and absorption may be normalized with respect to particle weight to give the corresponding parameters in cm^2 per gram of seed material, that is:

$$b_e = \sigma_e / \rho v \tag{12}$$

$$b_s = \sigma_s / \rho v \tag{13}$$

$$b_a = \sigma_a / \rho v = (\sigma_e - \sigma_s) / \rho v \tag{14}$$

where ρ is the mass density and V the volume of the seed particles.

Results of Mie Calculations

Mie calculations were performed to determine the effect of wavelength and particle size on the extinction, absorption, and scattering parameters of metal particles which might be used as seeding materials in rocket engines. Refractive index data required for the calculations were obtained from Figs. 2 through 5 and from the literature. The data obtained from the literature for cobalt (Ref. 21), iron (Ref. 22), titanium (Ref. 21), vanadium (Ref. 23), and zirconium (Ref. 21) are graphically illustrated in Figs. 6 through 10. The extinction and absorption parameters of small spherical particles made from these materials were calculated as a function of wavelength for various particle radii between 0.01 and 1.0μ. Theoretical results obtained using complex indices obtained from the literature are illustrated in Figs. 11 through 15. The results for cobalt (see Fig. 6) below a wavelength of approximately 2.5μ were previously reported in Ref. 10, while those above 2.5μ were computed as part of the current investigation. The results for iron, titanium, vanadium, and zirconium, except for a few points, represent the results of new calculations.

The results of Mie calculations made using the data of Figs. 2 through 5 are plotted in Figs. 16 through 19. A comparison of the absorption parameters of molybdenum particles ($R = 0.05$ and 0.50μ) based on refractive indices measured at UARL and refractive indices reported in Ref. 10 is given in Fig. 20. A similar comparison is graphically made in Fig. 21 for tungsten particles.

A graphical summary of the spectral absorption parameters of particles made from all nine materials studied during the current investigation is presented in Fig. 22 for wavelengths between 0.2 and 1.0μ and for particles having radii of 0.05μ. Similar results are presented in Fig. 23 for wavelengths between 1.0 and 20.0μ. As is evident in Fig. 22, the maximum calculated absorption parameter of $4.5 \times 10^4 cm^2/gm$ occurs at a wavelength of approximately 0.42μ- and 0.05μ-radius nickel particles.

Rosseland Mean Opacity Parameter of Tungsten Particles

The Rosseland mean opacity parameter is given by the following equation (Ref. 27):

$$b_R = \frac{\int_0^\infty \frac{dB_\omega}{dT}\, d\omega}{\int_0^\infty \frac{1}{b_a\,(1 - e^{-hc\omega/k'T})} \frac{dB_\omega}{dT}\, d\omega} \tag{15}$$

where the black-body function, B_ω, is given by:

$$B_\omega = \frac{2hc^2\omega^3}{(e^{hc\omega/k'T} - 1)} \tag{16}$$

Equation (15) was evaluated early in the program before the refractive index data from Fig. 5 were available for computation of the spectral absorption parameters. Therefore, determination of the Rosseland mean opacity parameter of tungsten particles ($R = 0.05\mu$) was based on the calculated spectral absorption parameters reported for this material at wavelengths between 0.4 and 4.0μ in Ref. 10. (The complex refractive index of tungsten used to calculate these spectral absorption parameters were reported in Ref. 25.) These spectral absorption parameter results from Ref. 10 are shown as a solid line in Fig. 24. In order to evaluate Eq. (15), it was necessary to extrapolate the absorption parameter results from Ref. 10 below a wave number of 2500 cm^{-1} ($\lambda > 4.0\mu$) and above a wave number of 25,000 cm^{-1} ($\lambda < 0.4\mu$). The extrapolated values of the absorption parameter are illustrated by dashed lines in Fig. 24. Also shown in Fig. 24 are the absorption parameter results based on the complex refractive index data from Fig. 5. (As previously noted, these results were not available when Eq. (15) was evaluated.) The extrapolated absorption parameter at wave numbers above 25,000 cm^{-1} ($\lambda < 0.4\mu$) shown in Fig. 24 is in fair agreement with the calculated absorption parameter based on the refractive index data from Fig. 5.

The Rosseland mean opacity results for 0.05-micron-radius tungsten particles are shown in Fig. 25. Note that the absorption parameter of tungsten used in the evaluation of Eq. (15) was based on refractive index data obtained at a temperature of approximately 300 K. Thus, the variation of the Rosseland mean opacity parameter with temperature shown in Fig. 25 is due to the variation of weighting function, dB_ω/dT and the stimulated emission factor, $(1 - e^{-hc\omega/kT})$ with temperature. As is evident in Fig. 25, the Rosseland mean opacity parameter of 0.05-micron-radius tungsten particles varies from a value of approximately 80 cm^2/gm at a temperature of 1600 K to a value of approximately 900 cm^2/gm at a temperature of 5600 K (approximate melting point of tungsten).

At a temperature of 5600 K, approximately 95 percent of the energy radiated by a black body is at wave numbers below about 25000 cm^{-1}, while at a temperature of 1600 K, almost all the black-body energy is at wave numbers less than 25000 cm^{-1}. Therefore, re-evaluation of Eq. (15) incorporating the spectral absorption parameter computed on the basis of the refractive index data from Fig. 5 would not appreciably alter the Rosseland mean opacity parameter shown in Fig. 25.

REFERENCES

1. Weinstein, H., and R. Ragsdale: The Coaxial Flow Reactor - A Gaseous Nuclear Rocket Concept. ARS Preprint 1518-60, presented at the ARS 15th Annual Meeting, Washington, D. C., December 1960.

2. Barré, J. J.: Contribution to the Problem of the Nuclear Rocket Engine. Proceedings of the VIII International Astronautical Congress, Barcelona, 1957, Springer-Verlag, Berlin, 1958, pp. 1-14.

3. Lanzo, C. D., and R. G. Ragsdale: Experimental Determination of Spectral and Total Transmissivities of Clouds of Small Particles. NASA Technical Note D-1405, September 1962.

4. Marteney, P. J., and N. L. Krascella: Theoretical and Experimental Investigations of Spectral Opacities of Mixtures of Hydrogen and Diatomic Gases. Air Force Systems Command Report RTD-TDR-63-1102 prepared by UAC Research Laboratories, November 1963.

5. Lanzo, C. D., and R. G. Ragsdale: Heat Transfer to a Seeded Flowing Gas from an Arc Enclosed by a Quartz Tube. NASA Technical Memorandum X-52005, June 1964.

6. Marteney, P. J.: Experimental Investigation of the Opacity of Small Particles. UAC Research Laboratories Report C-910092-2 prepared under Contract NASw-847, September 1964. (Also issued as NASA report CR-211)

7. McAlister, J. Andrew, Edward Y. H. Keng, and Clyde Orr, Jr.: Heat Transfer to a Gas Containing a Cloud of Particles. Prepared for National Aeronautics and Space Administration Contract NsG-273-62, July 30, 1965.

8. Love, T. J., and J. F. Beattie: Experimental Determination of Thermal Radiation Scattering by Small Particles. Aerospace Research Laboratories Report ARL 65-110, June 1965.

9. Mie, G. Annalen der Physik, Vol. 30, 1919.

10. Krascella, N. L.: Theoretical Investigation of the Absorption and Scattering Characteristics of Small Particles, UAC Research Laboratories Report C-910092-1 prepared under Contract NASw-847, September 1964. (Also issued as NASA Report CR-210.)

11. Handbook of Chemistry and Physics, Chemical Rubber Publishing Co., Cleveland, 1964.

12. Gray, D. E.: American Institute of Physics Handbook. McGraw-Hill Book Company, New York, 1963.

13. Simon, Ivan: Spectroscopy in Infrared by Reflection and Its Use for Highly Absorbing Substances. Journal of the Optical Society of America, Vol. 41, No. 5, May 1951.

14. Waldron, J. P., and D. W. Juenker: Optical Properties of Clean Molybdenum. Journal of the Optical Society of America, Vol. 54, No. 2, February 1964.

15. Huebner, R. H., E. T. Arakawa, R. A. MacRae, and R. N. Hamm: Optical Constants of Vacuum-Evaporated Silver Films. Journal of the Optical Society of America, Vol. 54, No. 12, December 1964.

16. Mertens, Frederick P., Paul Theroux, and Robert C. Plumb: Some Observations on the Use of Elliptically Polarized Light to Study Metal Surfaces. Journal of the Optical Society of America, Vol. 53, No. 7, July 1963.

17. McCrackin, Frank L., Elio Passaglia, Robert B. Stromberg, and Harold L. Steinberg: Measurement of the Thickness and Refractive Index of Very Thin Films and the Optical Properties of Surfaces by Ellipsometry. NBS Journal of Research, Vol. 67A, No. 4, August 1963.

18. Mertens, Frederick P., and Robert C. Plumb: Determining Optical Constants of Metals by Reflection of Elliptically Polarized Light. Journal of the Optical Society of America, Vol. 54, No. 8, August 1964.

19. Dettorre, J. F., T. G. Knorr, and D. A. Vaughan: Application of Ellipsometry to the Study of Phenomena on Surfaces Prepared in Ultrahigh Vacuum, in Passaglia, E., et al (eds.), Ellipsometry in the Measurement of Surfaces and Thin Films. National Bureau of Standards, Washington, D. C., September 1964.

20. McCrackin, Frank L., and James P. Colson: A Fortran Program for Analysis of Ellipsometer Measurements and Calculation of Reflection Coefficients from Thin Films. National Bureau of Standards, Technical Note 242, May 1964.

21. Kirillova, M. M., and B. A. Charikov: Study of the Optical Properties of Transition Metals. Optics and Spectroscopy, Vol. 17, No. 2, August 1964.

22. Yolken, H. T., and J. Kruger: Optical Constants of Iron in the Visible Region. Journal of the American Optical Society, Vol. 55, No. 7, July 1965.

23. G. A. Bolotin, et al: Optical Properties of Titanium and Vanadium in the Infrared Range of the Spectrum. Physics of Metals and Metallography, Vol. 13, No. 6, 1962.

24. Kirillova, M. M., and B. A. Charikov: Optical Properties of Titanium in the Quantum Transition Range. Physics of Metals and Metallography, Vol. 15, No. 2, 1963.

25. Roberts, S.: Optical Properties of Nickel and Tungsten and Their Interpretations According to Drude's Formula. Physical Review, Vol. 114, No. 1, April 1959.

26. Archer, R. J.: Optical Constants of Germanium. Physical Review, Vol. 110, No. 2, April 1958.

27. Chandrasekhar, S.: An Introduction to the Study of Stellar Structure. Dover Publication, Incorporated, New York, 1957.

28. McCrackin, F. L., and J. P. Colson: Computational Techniques for the Use of the Exact Drude Equations in Reflection Problems, in Passaglia, E., et al (eds.), Ellipsometry in the Measurement of Surfaces and Thin Films. National Bureau of Standards, Washington, D. C., September 1964.

29. Zaininger, K. H., and A. G. Revesz: Ellipsometry--A Valuable Tool in Surface Research. RCA Review, March 1964.

30. Hall, A. C.: Experimental Determination of the Optical Constants of Metals. Journal of the Optical Society of America, Vol. 55, No. 8, 911-915, August 1965.

LIST OF SYMBOLS

a	Reduced value of azimuthal setting of analyzer, deg
a_m	Mie coefficient, see Eq. (8)
a_ω	Spectral absorption coefficient, cm^{-1}
A	Experimental value of azimuthal setting of analyzer, deg
b_a	Absorption parameter, cm^2/gm
b_e	Extinction parameter, cm^2/gm
b_m	Mie coefficient, see Eq. (9)
b_R	Rosseland mean opacity parameter, cm^2/gm
b_s	Scattering parameter, cm^2/gm
B_ω	Black-body function, see Eq. (16)
C	Velocity of light, 2.9979×10^{10} cm/sec
h	Planck's constant, 6.6237×10^{-27} erg-sec
$h_m^{(2)}(\ )$	Spherical Hankel function
i	$\sqrt{-1}$
I	Intensity of light after passage through sample, arbitrary units
I_o	Intensity of light before passage through sample, arbitrary units
$j_m(\ )$	Spherical Bessel function
k'	Boltzmann constant, 1.3802×10^{-16} erg/deg K
k	Imaginary part of refractive index
n, n'	Real part of refractive index
N	Complex refractive index, $N = n - ik$

$\bar{N}$	Relative refractive index, see Eq. (10)
N_1	Refractive index of particle
N_2	Refractive index of matrix or medium
p	Reduced value of azimuthal setting of polarizer, deg
P	Experimental value of azimuthal setting of polarizer, deg
r	Reflection coefficient of light incident on surface
R	Particle radius, microns
Re	Real part of a complex quantity
T	Temperature, deg K
V	Particle volume, cm^3
x	Sample thickness, cm

Greek Letters

α	Relative size parameter, see Eq. (7)
Δ	Phase difference introduced between parallel and perpendicular plane light waves upon reflection, deg
θ	Phase difference introduced by compensator, deg
λ	Wavelength, Angstroms or microns
ρ	Mass density, gm/cm^3
σ_a	Absorption cross-section, cm^2/particle
σ_e	Extinction cross-section, cm^2/particle
σ_s	Scattering cross-section, cm^2/particle
ϕ, ϕ'	Angle of incidence of light relative to normal to sample, deg
χ	Angle of refraction of light relative to normal to sample, deg

ψ	Arc tan of ratio of reflection coefficients of parallel and perpendicular plane light waves, deg
ω	Wave number, cm^{-1}

Subscripts

p	Plane of polarization parallel to normal to surface
s	Plane of polarization perpendicular to normal to surface

APPENDIX I

EQUATIONS RELATING THE COMPLEX REFRACTIVE INDEX TO EXPERIMENTAL QUANTITIES

The reflection coefficients of light polarized in planes parallel and perpendicular to the plane of incidence are given by the Fresnel equations (Ref. 13):

$$r_p = \frac{\tan^2(\phi - \chi)}{\tan^2(\phi + \chi)}, \qquad r_s = \frac{\sin^2(\phi - \chi)}{\sin^2(\phi + \chi)} \tag{I-1}$$

According to Snell's law,

$$\sin \phi = N \sin \chi \tag{I-2}$$

when N is complex and defined as:

$$N = n - ik \tag{I-3}$$

By proper manipulation of Eqs. (I-1) through (I-3), reflection coefficients can be related to the complex refractive index (Ref. 13). However, the resulting equations lead more directly to a description of the experimentally observable quantities r_p and r_s in terms of n and k than to a reduction of the measured r_p and r_s to yield n and k. Therefore, it is the practice to solve for the reflection coefficients in the vicinity of anticipated ranges of the complex refractive index and solve for the single values of n and k by graphical interpolation.

In the ellipsometric method (Ref. 28), the quantity of interest is the ratio of the reflection coefficients of light polarized parallel and perpendicular to the plane of incidence,

$$r = r_p / r_s \tag{I-4}$$

where r_p and r_s are defined in Eq. (I-1). In terms of measurable quantities,

$$r = \tan \psi \, e^{i\Delta} \tag{I-5}$$

where ψ and Δ are related to a and p, the reduced experimental analyzer and polarizer settings, respectively, by

$$\psi = a \tag{I-6}$$

$$\Delta = 2p + 90^\circ \tag{I-7}$$

The complex refractive index may then be computed from the following equation (Refs. 28 and 29).

$$N = N_2 \tan \phi \left[1 - \frac{r \sin^2 \phi}{(r+1)^2} \right]^{1/2} \tag{I-8}$$

APPENDIX II

DATA REDUCTION AND PRECISION IN ELLIPSOMETER MEASUREMENTS

Reduction of Data

As indicated in APPENDIX I, the three quantities, ϕ, α, and ρ are necessary to specify n and k for a given wavelength. The angle of incidence, ϕ, is utilized directly in data reduction. The true values of ρ and α were found using the scheme shown in TABLE I, which summarizes the relationships between the experimental and reduced quantities for two orientations of the compensator. Note that two values of the analyzer settings, α_p and α_s, arise as a result of having the orientation of the polarizer plane of transmission nearer either the plane of incidence or the plane of the surface. Readings at each wavelength yielded α_p, α_s, and two values of ρ. The true value of α was taken as the average of α_p and α_s. Significant differences in α_p and α_s, which would arise from compensator retardation other than 90 deg, did not occur. Typical values for ρ and α are shown in Fig. 26.

A machine program (Ref. 20) was employed to compute the complex refractive index from the observed values of ρ and α. The principal equations are given in APPENDIX I. Input data included the refractive index (assumed real and equal to unity) of the surrounding medium, the angle of incidence, the average of the two ρ settings and the average of α_p and α_s. The machine program then computed a complex refractive index for each set of ρ and α values. The variations of n and k with the analyzer setting for various polarizer settings are shown in Figs. 27 and 28, respectively.

Discussion of Errors

Errors in ellipsometric measurements arise from many sources: improper alignment and orientation of components, failure to locate the true intensity minimum, improper compensator settings, wrong sample orientation, and human error in readout.

The established alignment procedure assured that the optical axis was in proper reference to the sample and that the polarizer and analyzer sides were properly oriented. The average error in polarizer orientation, with the analyzer fixed at 0 deg during alignment, was $\pm$ 0.03 deg. The compensator orientation was factory-set and was found to be within $\pm$ 0.02 deg of the desired position.

The minimum error which may be associated with the location of the minimum may be found by examination of Figs. 29 and 30, in which the effect of independent analyzer and polarizer rotations are shown. A minimum deflection of 0.05 intensity units could be distinguished; this corresponds to ± 0.15 deg. However, it is possible to estimate the minimum point more closely by passing through the minimum several times. It was found that several operators in succession could reproduce the same setting to ± 0.10 deg. The errors in the real and imaginary parts of the refractive index associated with errors of ± 0.15 deg in the polarizer and analyzer settings are approximately $n = \pm 0.02$ and $k = \pm 0.02$ when either p or a is held independently constant.

The effect of using a compensator yielding other than 90 deg retardation is to induce differences between a_p and a_s (Ref. 17). The calibration of the compensator was intended to eliminate this source of error. However, differences in p's and a's for different zones still occur. For example, see Fig. 26, in which the two values of p and a at each wavelength are obtained from different zones. This behavior has been observed previously and is ascribed to a non-removable instrumental error; averaging the settings from two zones is a satisfactory remedy (Ref. 17).

The effect of using a compensator retardation of other than 90 deg was determined; the results are shown in Fig. 31. Settings of p and a were obtained for several compensator settings; the a and p values from each of two zones were averaged, and the n and k were computed. It is shown that the error is negligible so long as the average of a_p and a_s is used. It is possible to calculate the compensator retardation by assuming that any difference between a_p and a_s is due to compensator error, according to the equation (Ref. 17)

$$a_p - a_s = (\theta - \pi/2) \cos 2p \tan 2\psi \qquad \text{(II-1)}$$

When this was done, the calculated compensator retardation corresponded extremely well to that expected on the basis of observed compensator calibration.

Alignment of the sample at 0 deg by reflecting the incident beam minimized orientation errors. Changes of ± 2 min from the aligned sample position yielded no change in the experimental parameters. One important aspect of sample orientation was, however, closely checked; this is the effect of angle of incidence on the calculated n and k. The magnitude of the effect is not well established (Refs. 18 and 30). To determine the effect, measurements were made at known angles of incidence of 60 to 80 deg on several metals. The results are shown in Fig. 32. It is evident that only a small effect occurs, and that the highest values of n and k are found for incident angles of 65 deg. The effect of misalignment and

consequent use of the wrong value of the angle of incidence was determined by computation; an error of 1 deg in the angle of incidence leads to errors of approximately 0.05 and 0.10 in n and k, respectively. Orientation errors as small as 5 min. were easily avoided; misalignment was not a significant source of error.

The human error in readout was reduced by plotting the experimentally observed values of ρ and σ, as shown in Fig. 26. Since a smooth curve is to be expected, misinterpretation of the true setting of ρ or σ can be recognized. Reading errors less than approximately 0.5 deg are not, however, readily identifiable as such, but will be reduced in effect by the zone-averaging process.

TABLE I

Relation of Polarizer and Analyzer Settings

to the True Values of P, α_p, and α_s

Zone	Compensator Orientation-Deg	P-Deg	A-Deg
1	- 45	p, $p + 180$	α_p, $\alpha_p + 180$
2	- 45	$p + 90$, $p + 270$	$180 - \alpha_s$, $360 - \alpha_s$
3	+ 45	$90 - p$, $270 - p$	α_s, $\alpha_s + 180$
4	+ 45	$180 - p$, $360 - p$	$180 - \alpha_p$, $360 - \alpha_p$

TABLE II

Organization of Figures

Material	Data Source on Refractive Index	Wavelength Interval, μ	Figures on Which Data Presented		
			Refractive Index	Absorption and Extinction Parameters	Rosseland Mean Opacity Parameter
Cobalt	Ref. 12 Ref. 21	0.231 - 2.25 2.5 - 20.0	6 6	11, 22, 23	
Hafnium	Present study	0.2 - 0.7	2	16, 22	
Iron	Ref. 22	0.367 - 0.692	7	12, 22	
Molybdenum	Present study Ref. 14	0.2 - 0.7 0.248 - 0.577	3 See Ref. 10	17, 20, 22	
Nickel	Present study	0.2 - 0.7	4	18, 22	
Titanium	Ref. 24 Ref. 21	0.475 - 4.0 2.5 - 20.0	8 8	13, 22, 23	
Tungsten	Present study Ref. 25	0.2 - 0.7 0.4 - 4.0	5 See Ref. 10	19, 21, 22, 24	25
Vanadium	Ref. 23	2.0 - 9.0	9	14, 23	
Zirconium	Ref. 21	2.5 - 17.0	10	15, 23	

SCHEMATIC DIAGRAM OF ELLIPSOMETER SHOWING PRINCIPAL COMPONENTS AND STATES OF POLARIZATION OF LIGHT

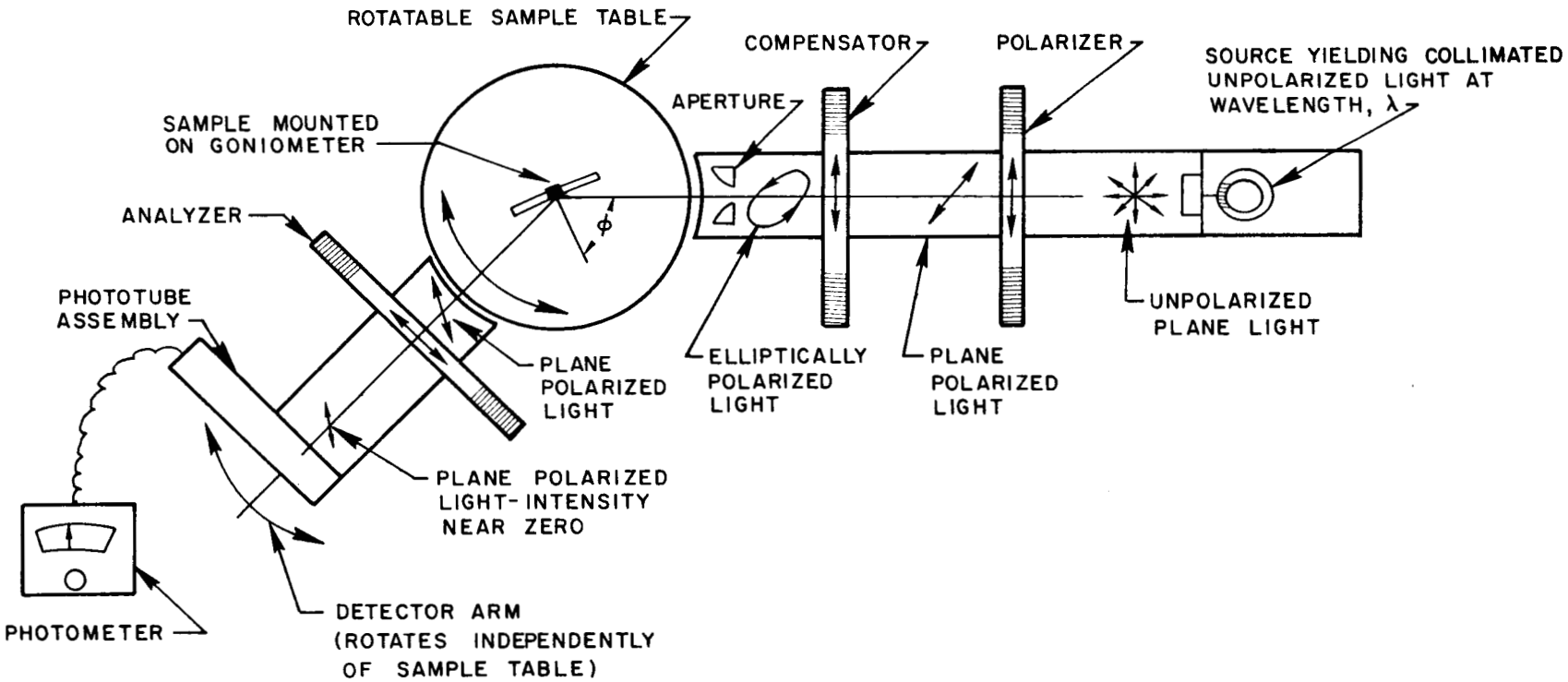

FIG. 1

EXPERIMENTALLY DETERMINED REAL AND IMAGINARY PARTS OF THE COMPLEX REFRACTIVE INDEX OF HAFNIUM BETWEEN 0.2μ AND 0.7μ

COMPLEX REFRACTIVE INDEX $N = n - ik$

FLAGS ON SYMBOLS INDICATE SUPERPOSITION OF DATA POINTS

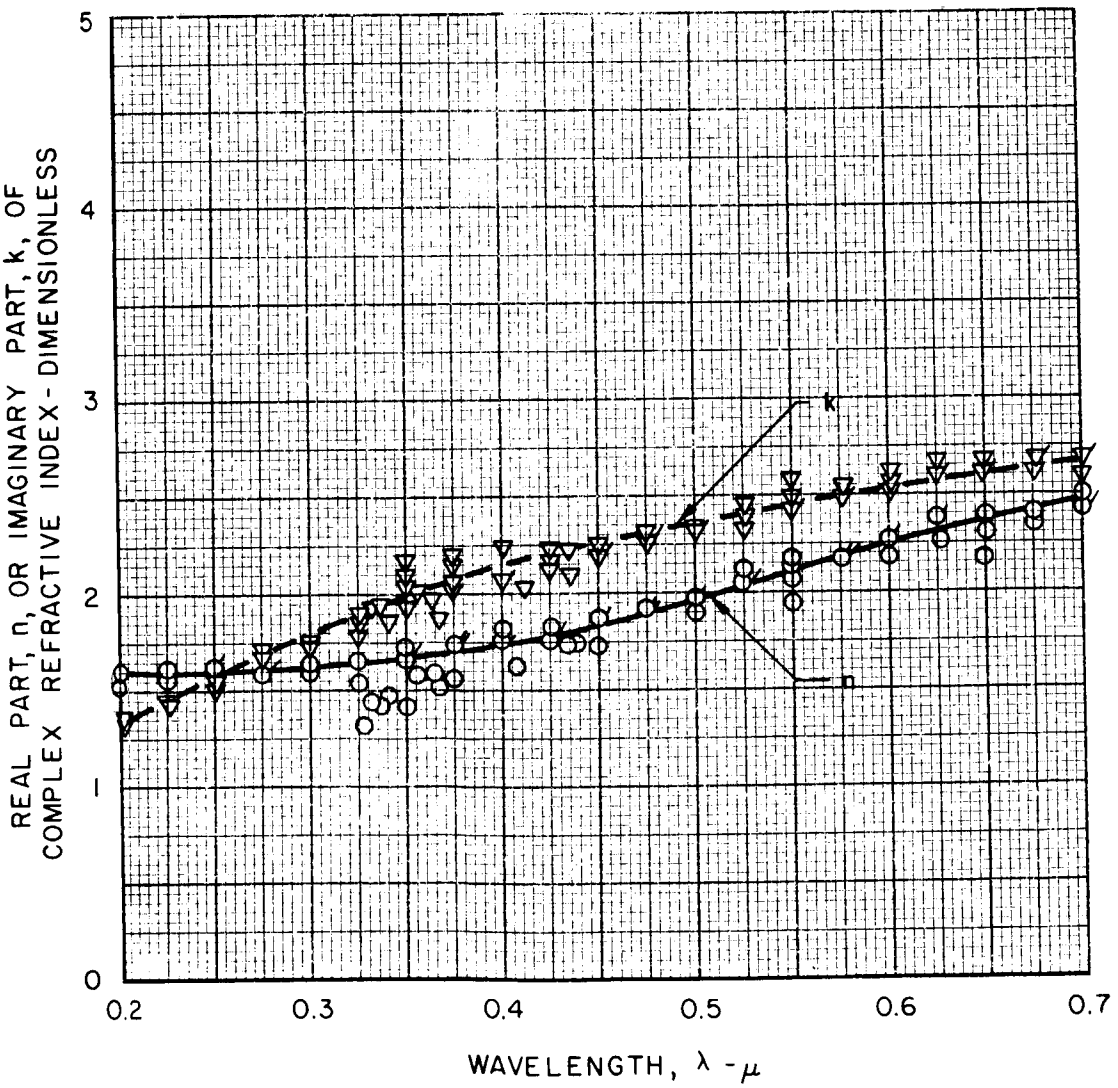

EXPERIMENTALLY DETERMINED REAL AND IMAGINARY PARTS OF THE COMPLEX REFRACTIVE INDEX OF MOLYBDENUM BETWEEN 0.2μ AND 0.7μ

COMPLEX REFRACTIVE INDEX $N = n - ik$

FLAGS ON SYMBOLS INDICATE SUPERPOSITION OF DATA POINTS

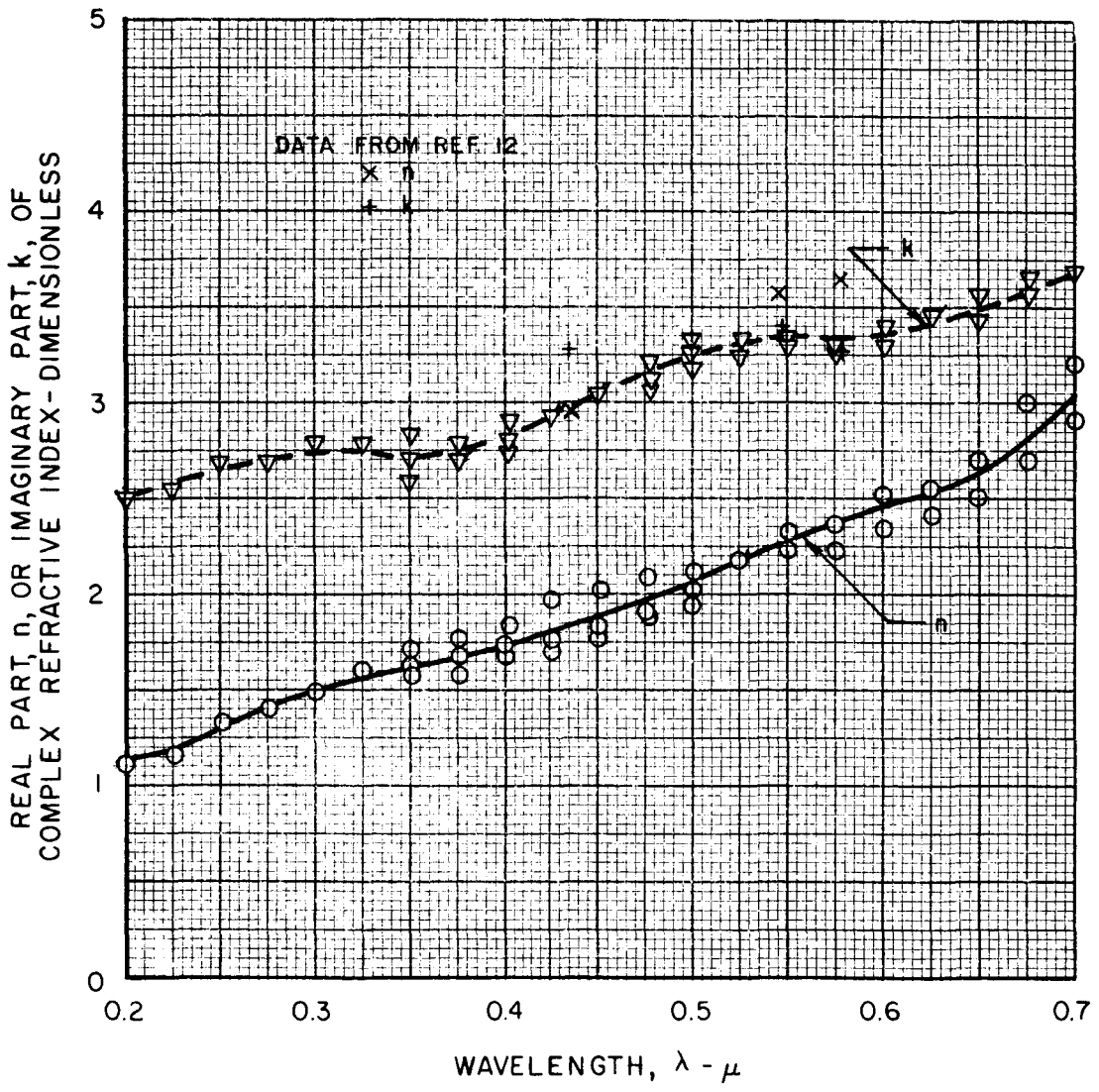

EXPERIMENTALLY DETERMINED REAL AND IMAGINARY PARTS OF THE COMPLEX REFRACTIVE INDEX OF NICKEL BETWEEN 0.2μ AND 0.7μ

COMPLEX REFRACTIVE INDEX N= n - ik
FLAGS ON SYMBOLS INDICATE SUPERPOSITION OF DATA POINTS

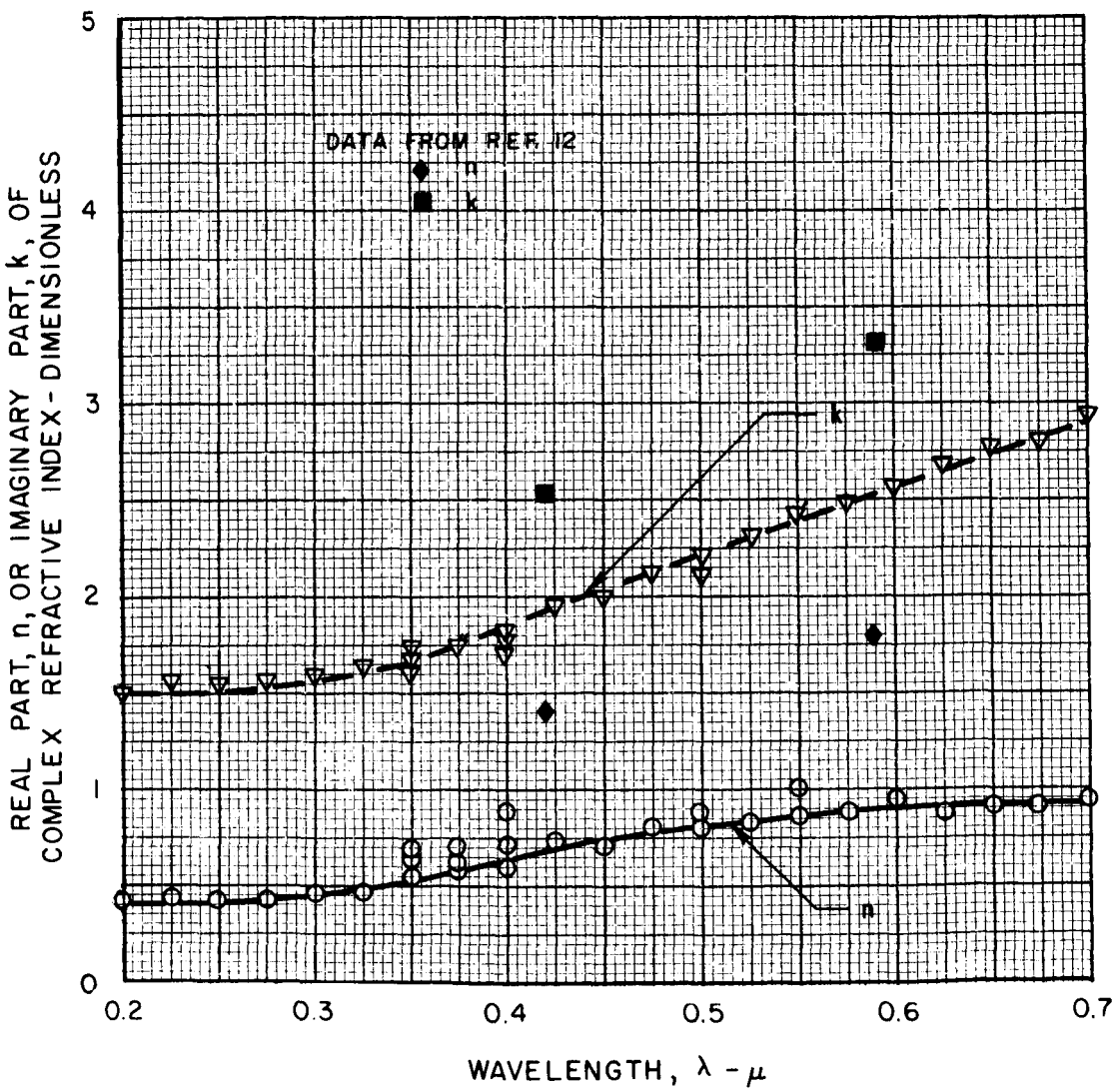

EXPERIMENTALLY DETERMINED REAL AND IMAGINARY PARTS OF THE COMPLEX REFRACTIVE INDEX OF TUNGSTEN BETWEEN 0.2μ AND 0.7μ

COMPLEX REFRACTIVE INDEX N= n - i k

FLAGS ON SYMBOLS INDICATE SUPERPOSITION OF DATA POINTS

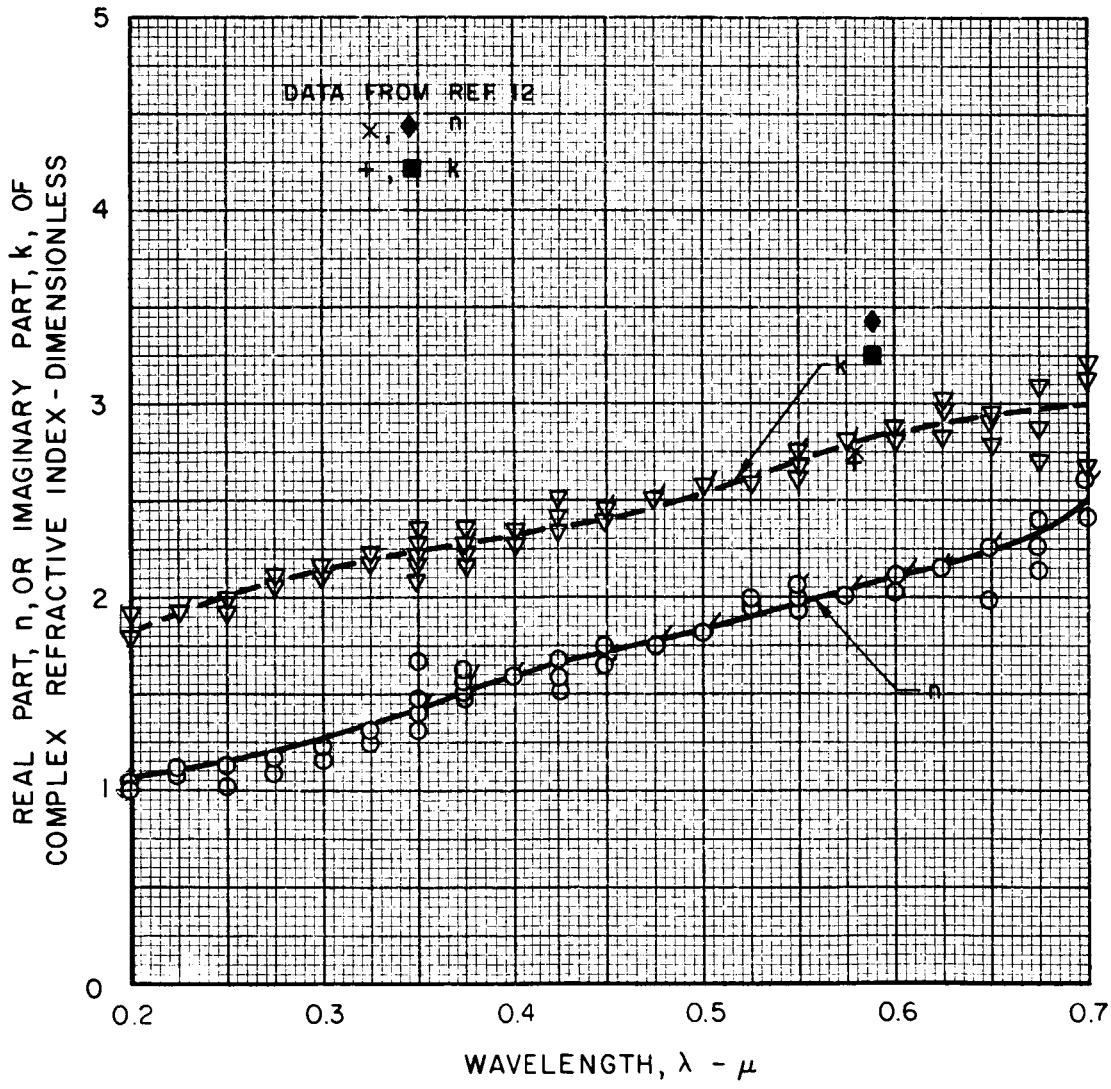

EFFECT OF WAVELENGTH ON THE REAL AND IMAGINARY PARTS OF THE REFRACTIVE INDEX OF COBALT

$N = n - ik$

O – DATA FROM REF. 21

x – DATA FROM REF. 12

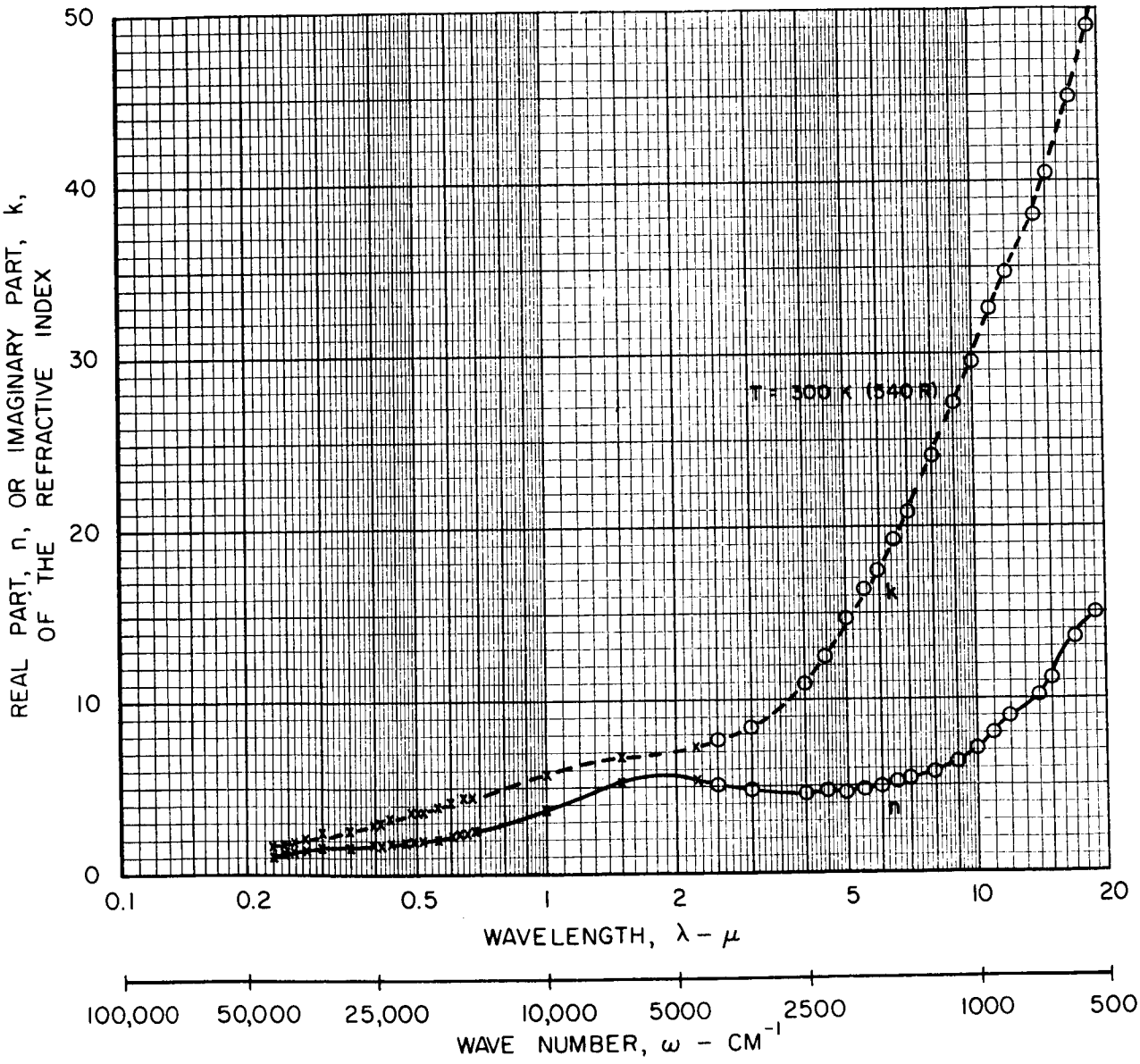

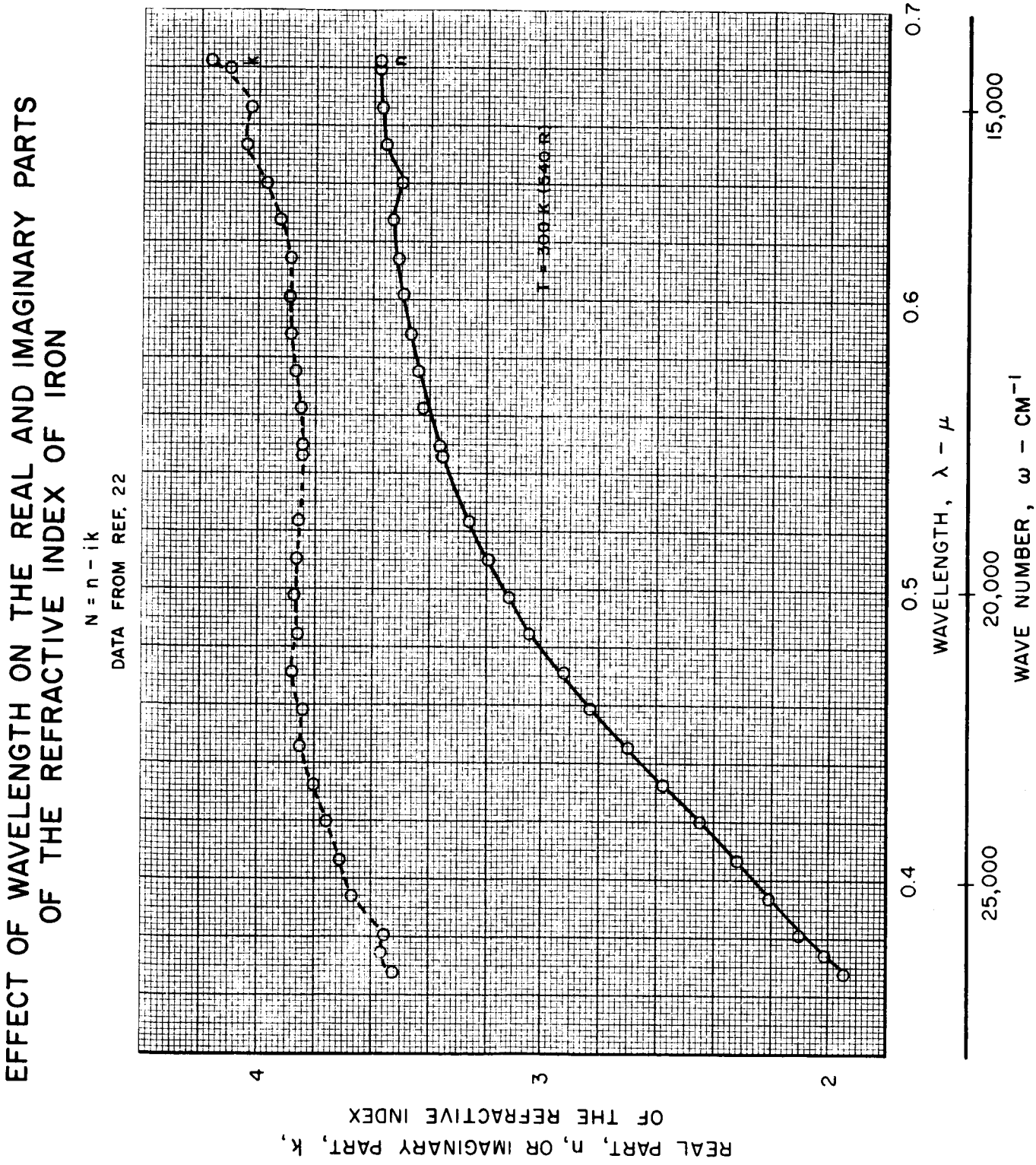
EFFECT OF WAVELENGTH ON THE REAL AND IMAGINARY PARTS
OF THE REFRACTIVE INDEX OF IRON
N = n - ik
DATA FROM REF. 22
k
n
T = 300 K (540 R)
4
3
2
REAL PART, n, OR IMAGINARY PART, k,
OF THE REFRACTIVE INDEX
0.4
0.5
0.6
0.7
WAVELENGTH, λ - μ
25,000
20,000
15,000
WAVE NUMBER, ω - CM⁻¹

EFFECT OF WAVELENGTH ON THE REAL AND IMAGINARY PARTS OF THE REFRACTIVE INDEX OF TITANIUM

$N = n - ik$

O – DATA FROM REF. 21

x – DATA FROM REF. 24

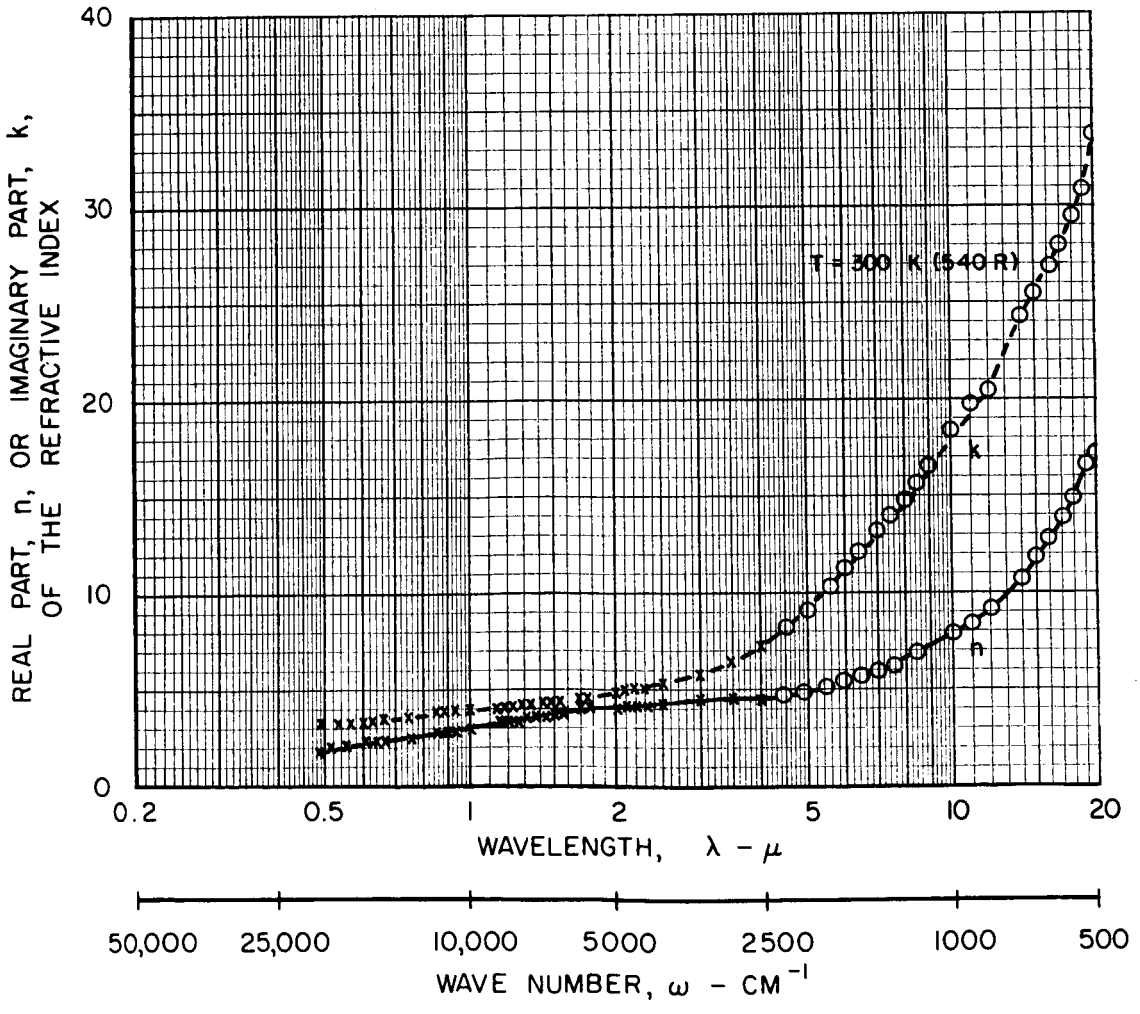

EFFECT OF WAVELENGTH ON THE REAL AND IMAGINARY PARTS OF THE REFRACTIVE INDEX OF VANADIUM

$N = n - ik$

DATA FROM REF. 23

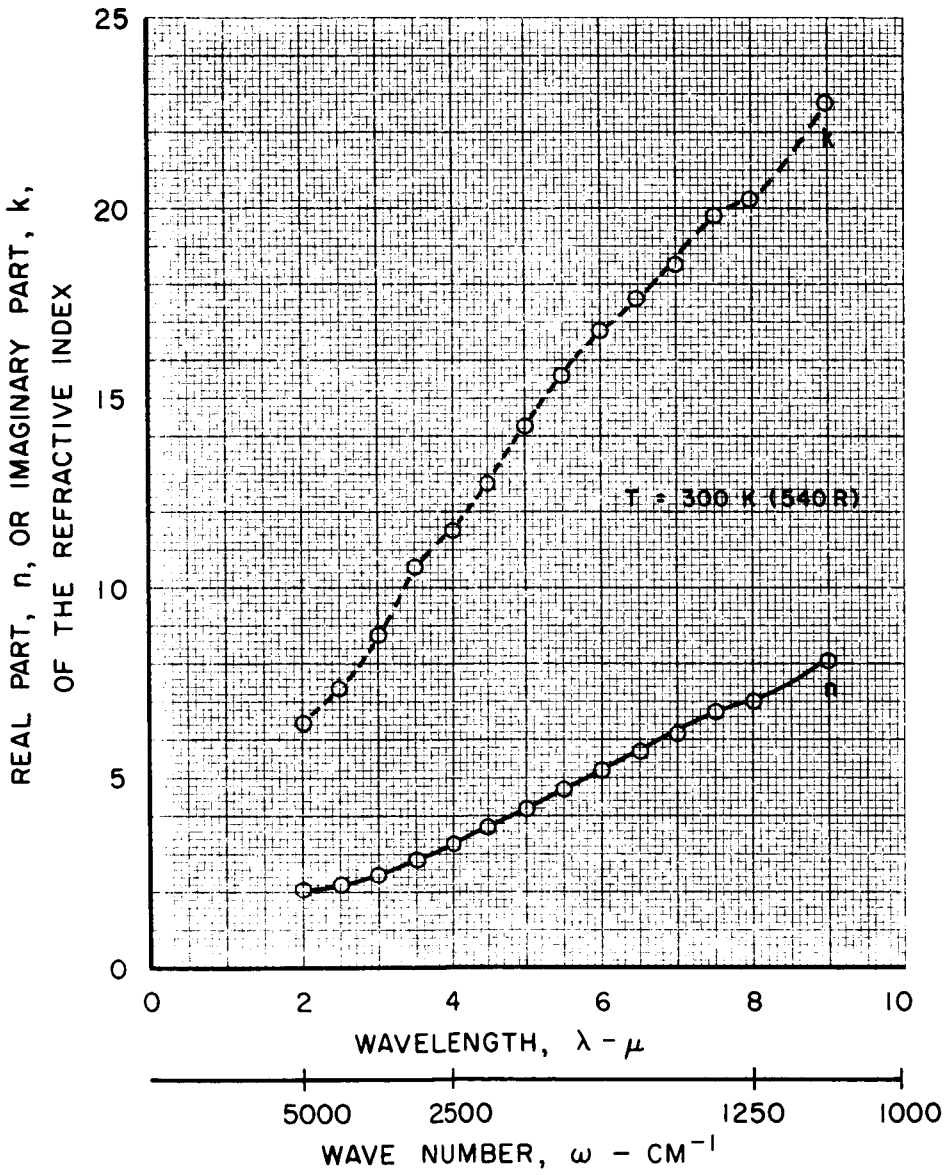

EFFECT OF WAVELENGTH ON THE REAL AND IMAGINARY PARTS OF THE REFRACTIVE INDEX OF ZIRCONIUM

$N = n - ik$

DATA FROM REF. 21

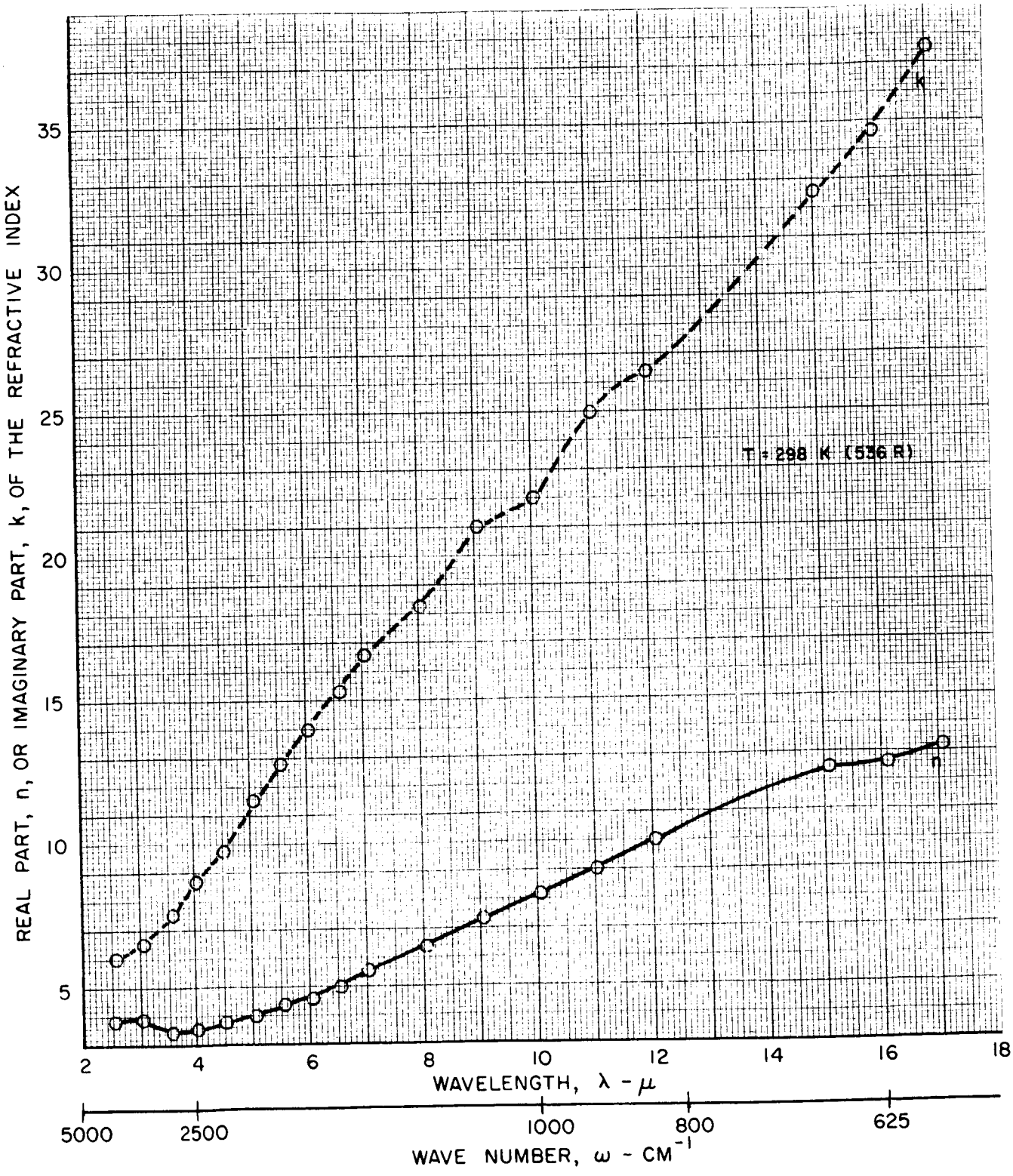

EFFECT OF WAVELENGTH ON THE EXTINCTION AND ABSORPTION PARAMETERS OF SPHERICAL COBALT PARTICLES

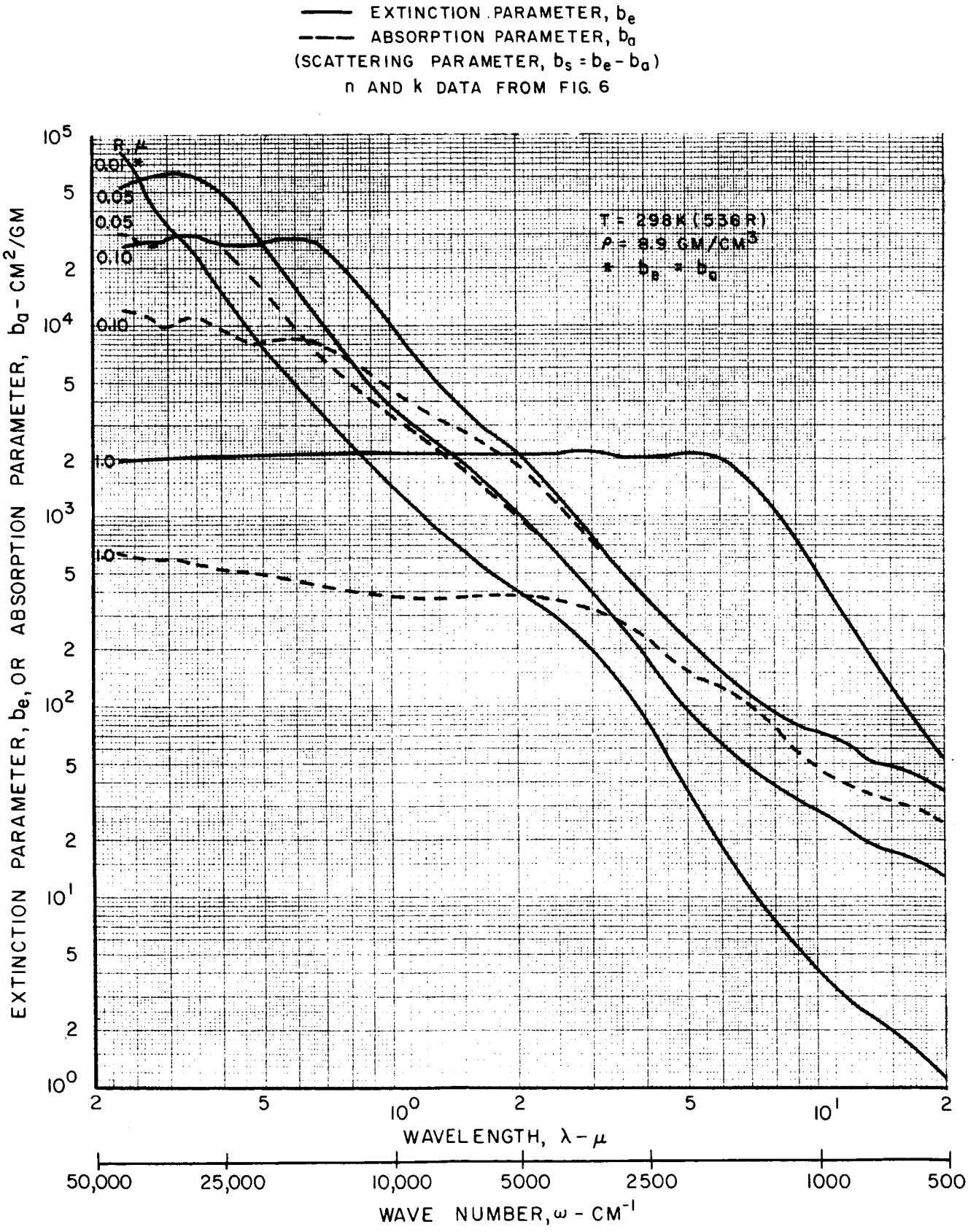

EFFECT OF WAVELENGTH ON THE EXTINCTION AND ABSORPTION PARAMETERS OF SPHERICAL IRON PARTICLES

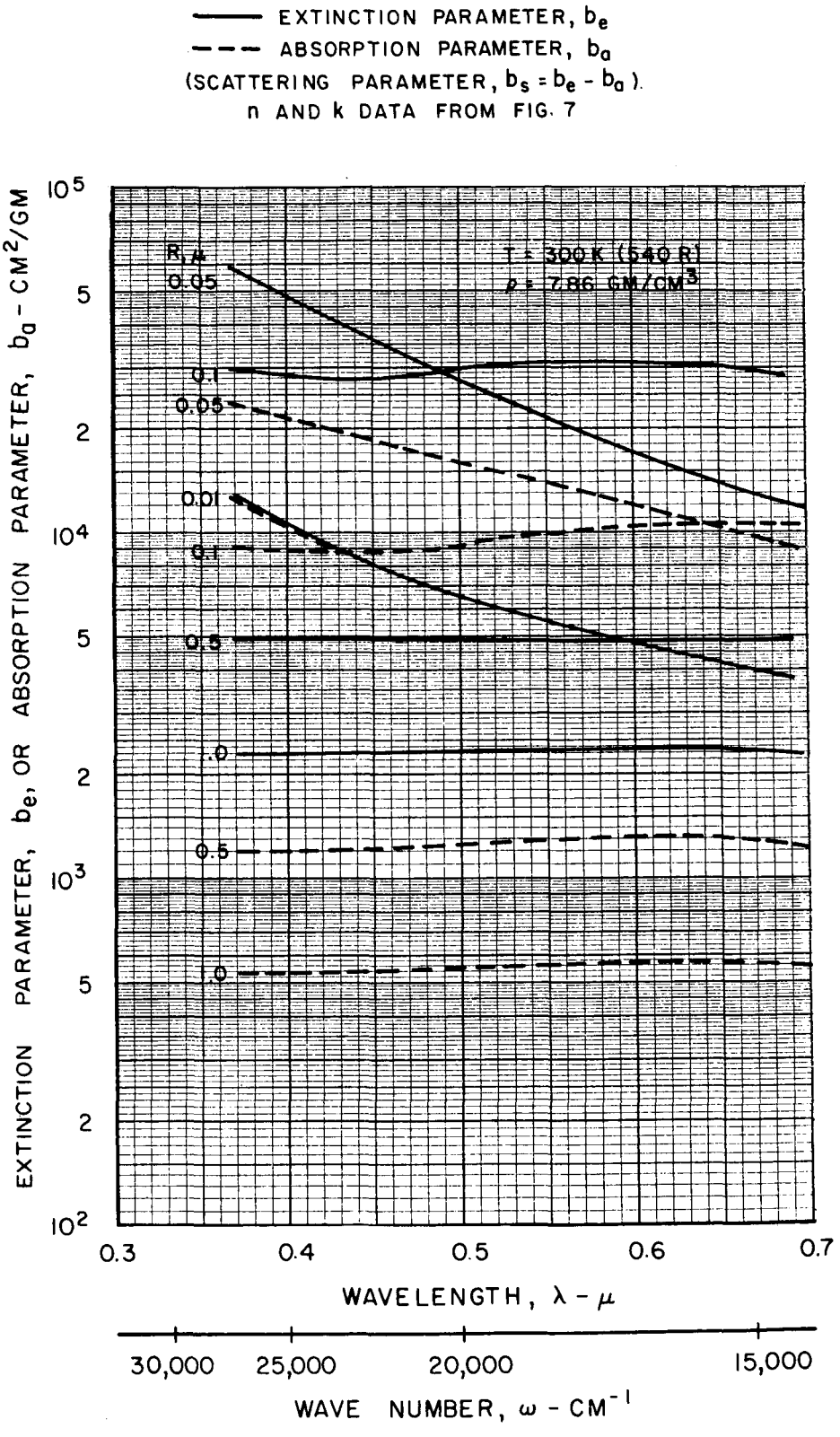

EFFECT OF WAVELENGTH ON THE EXTINCTION AND ABSORPTION PARAMETERS OF SPHERICAL TITANIUM PARTICLES

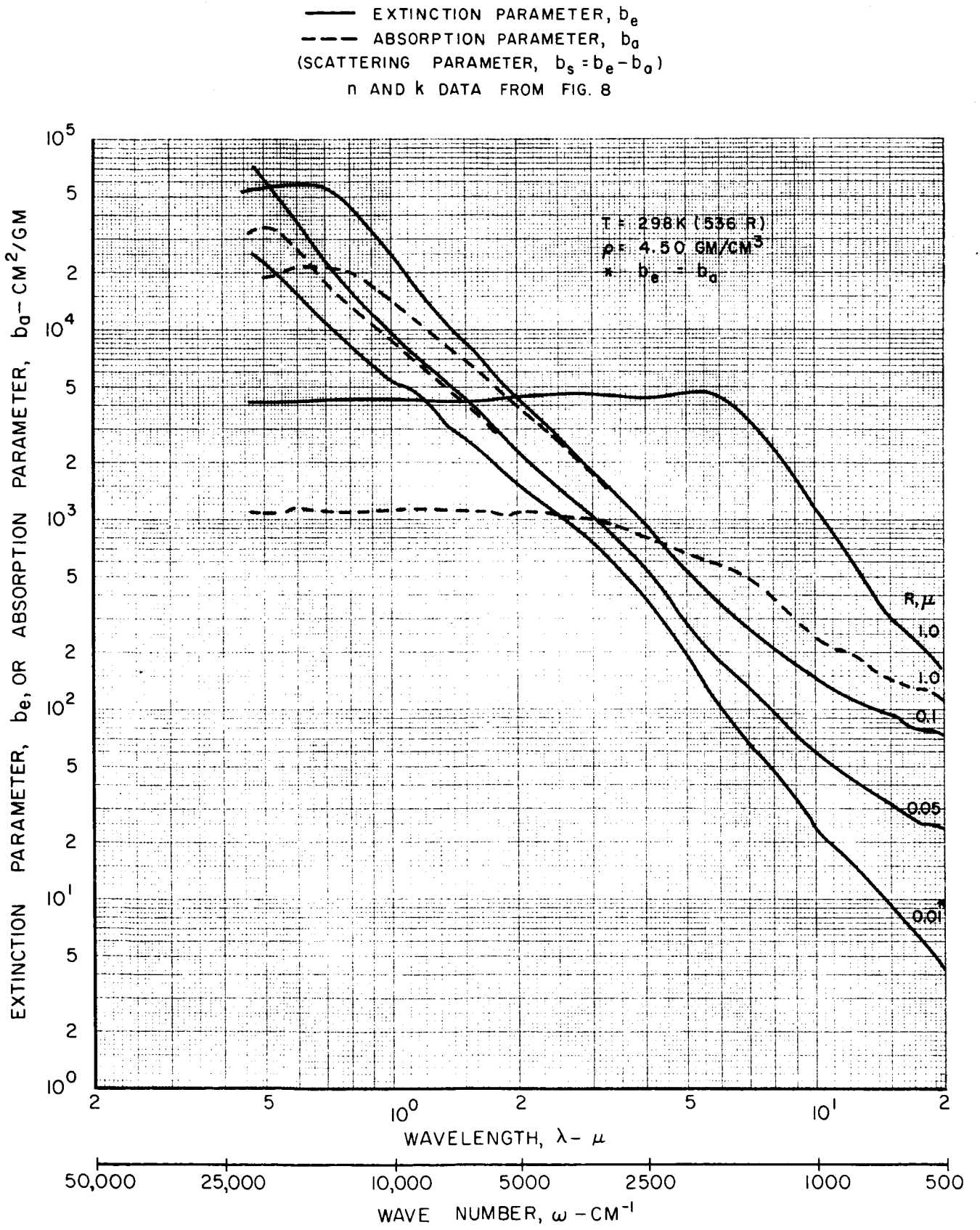

EFFECT OF WAVELENGTH ON THE EXTINCTION AND ABSORPTION PARAMETERS OF SPHERICAL VANADIUM PARTICLES

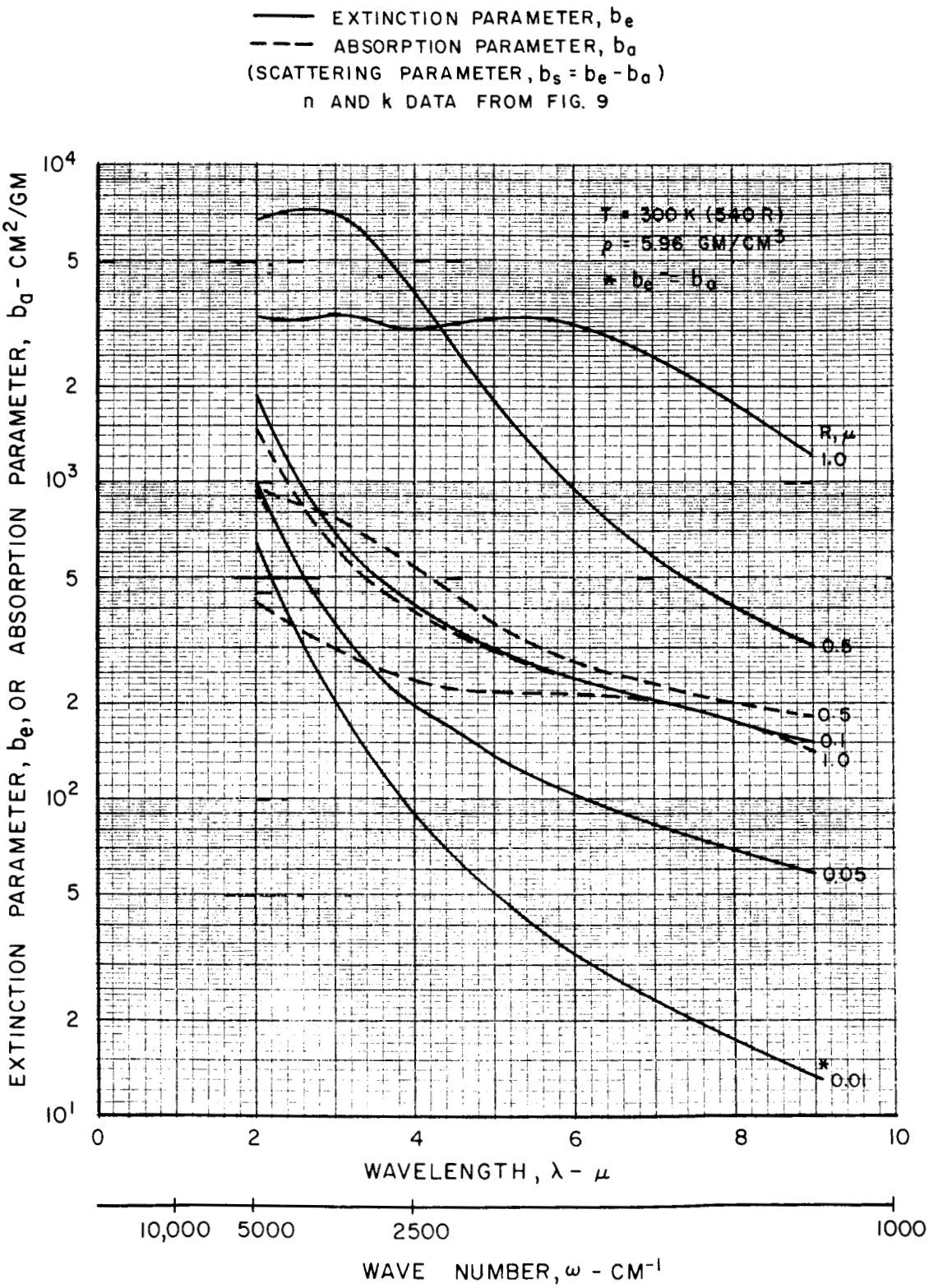

EFFECT OF WAVELENGTH ON THE EXTINCTION AND ABSORPTION PARAMETERS OF SPHERICAL ZIRCONIUM PARTICLES

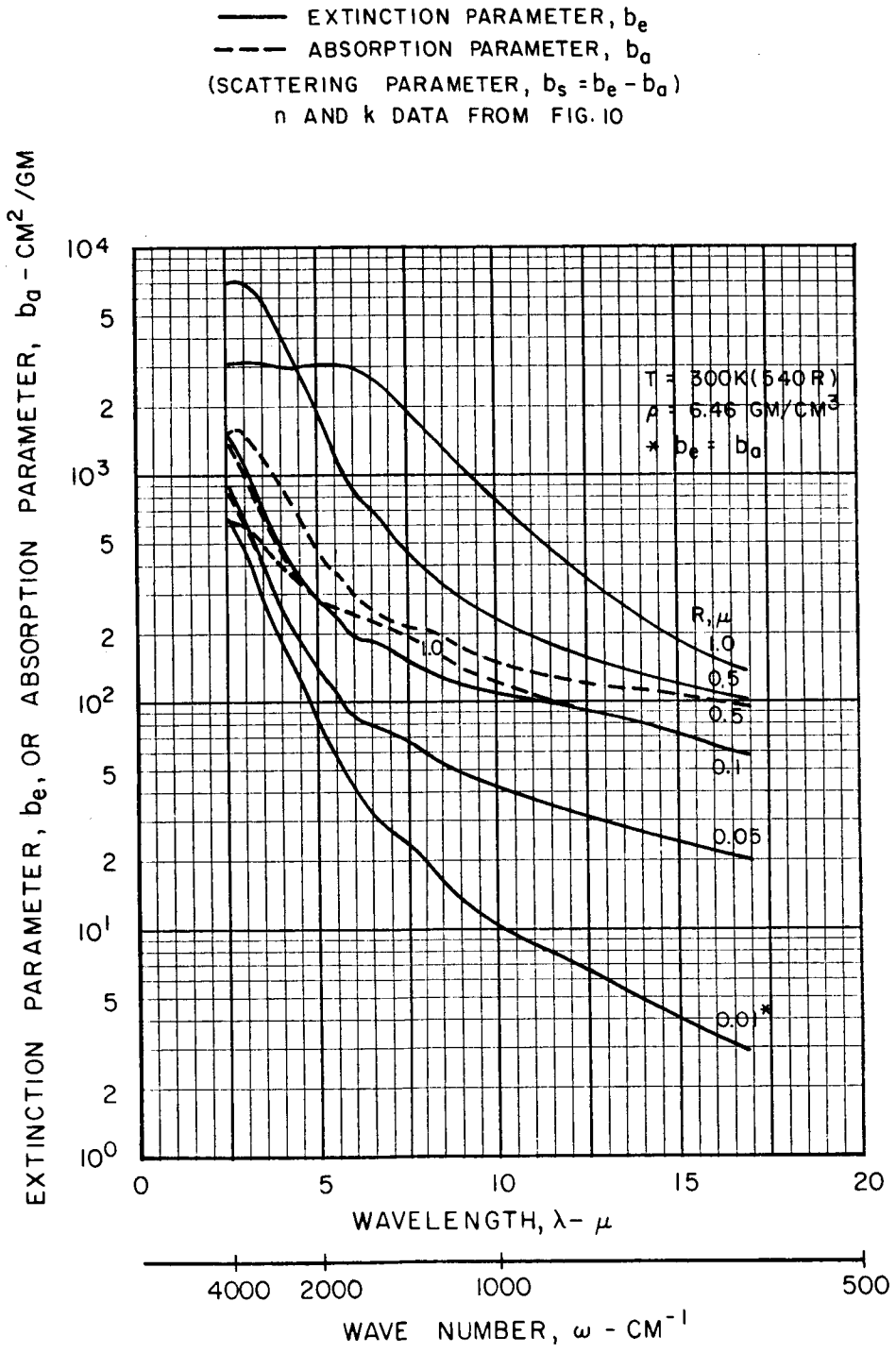

EFFECT OF WAVELENGTH ON THE EXTINCTION AND ABSORPTION PARAMETERS OF SPHERICAL HAFNIUM PARTICLES

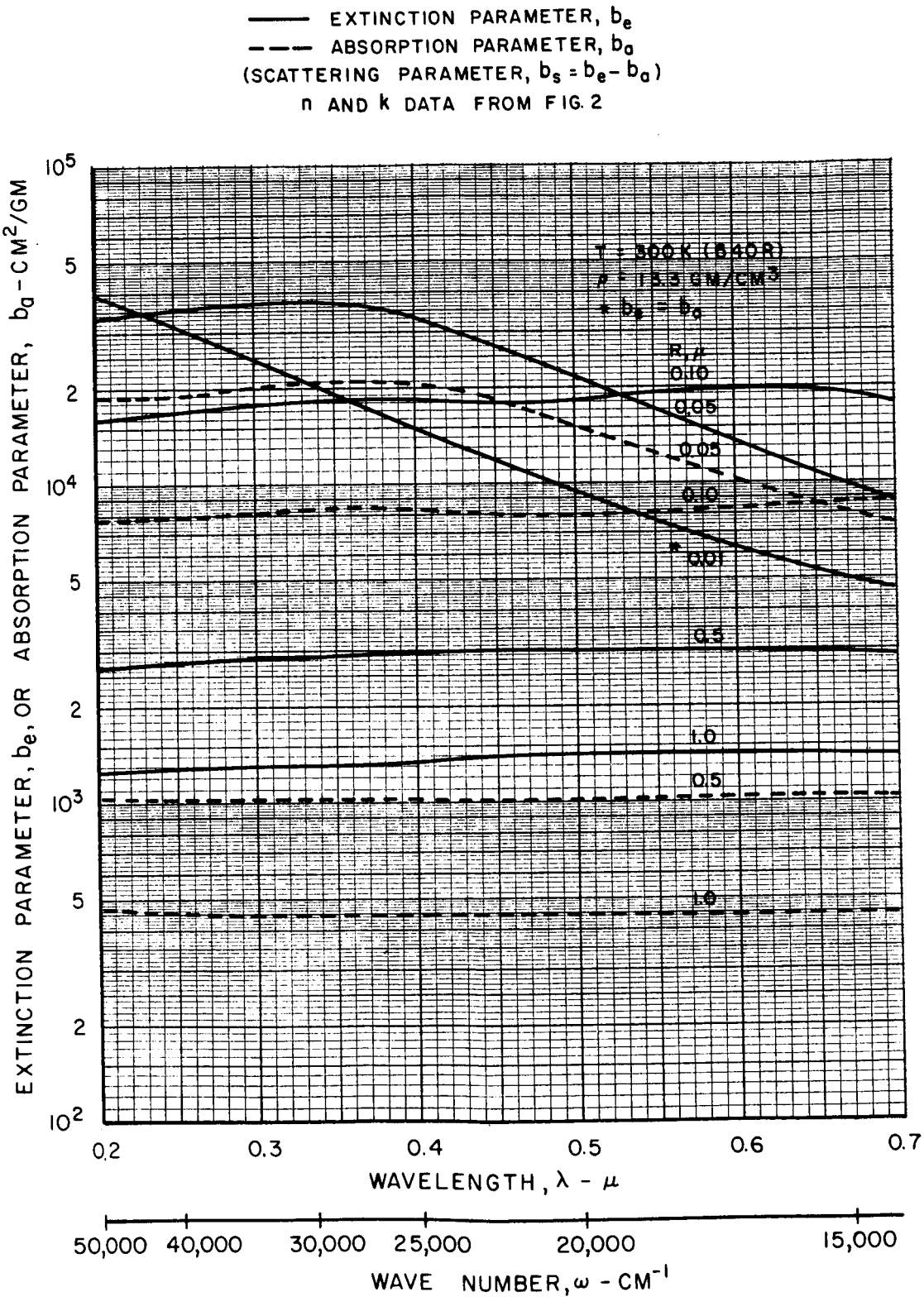

EFFECT OF WAVELENGTH ON THE EXTINCTION AND ABSORPTION PARAMETERS OF SPHERICAL MOLYBDENUM PARTICLES

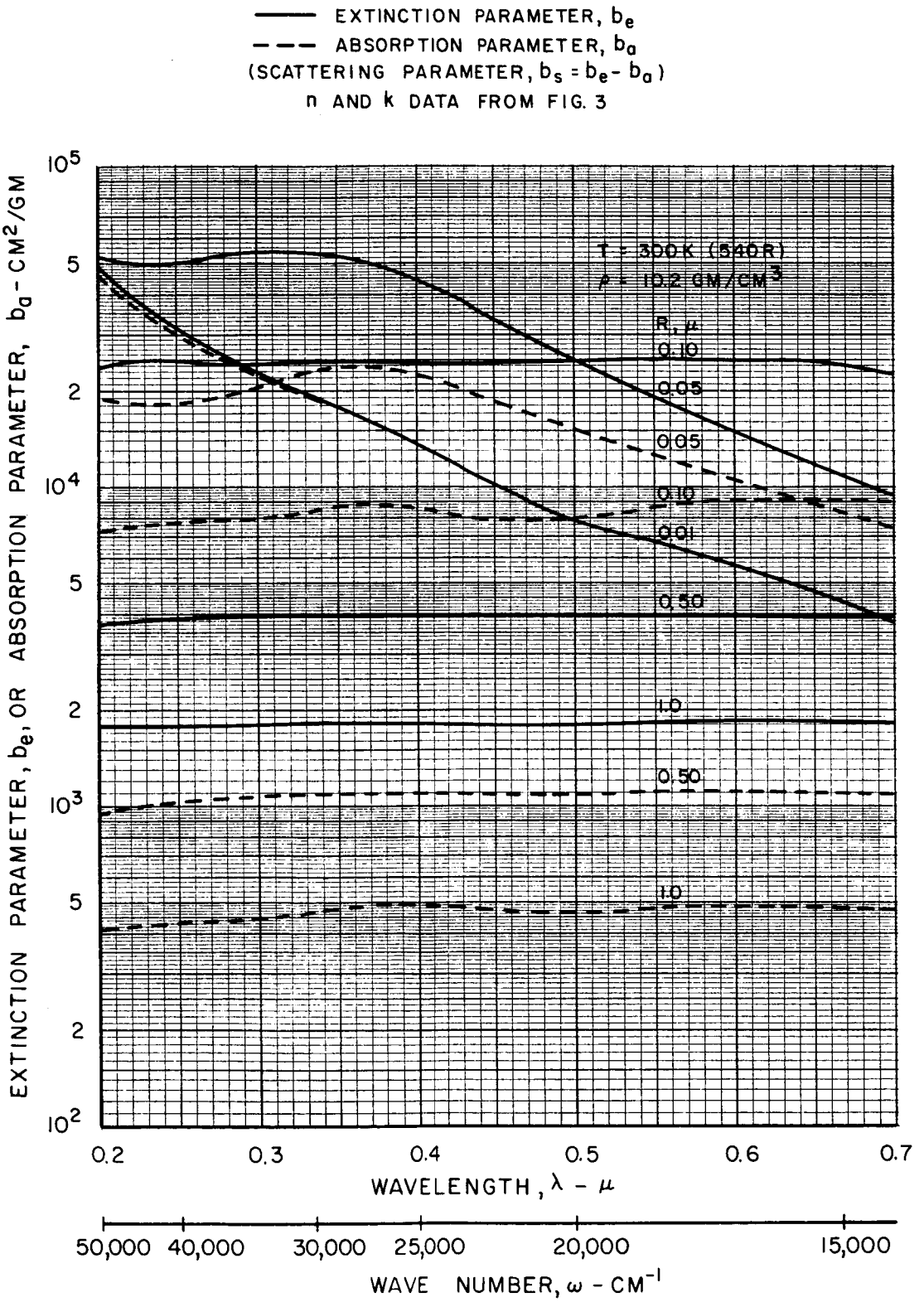

EFFECT OF WAVELENGTH ON THE EXTINCTION AND ABSORPTION PARAMETERS OF SPHERICAL NICKEL PARTICLES

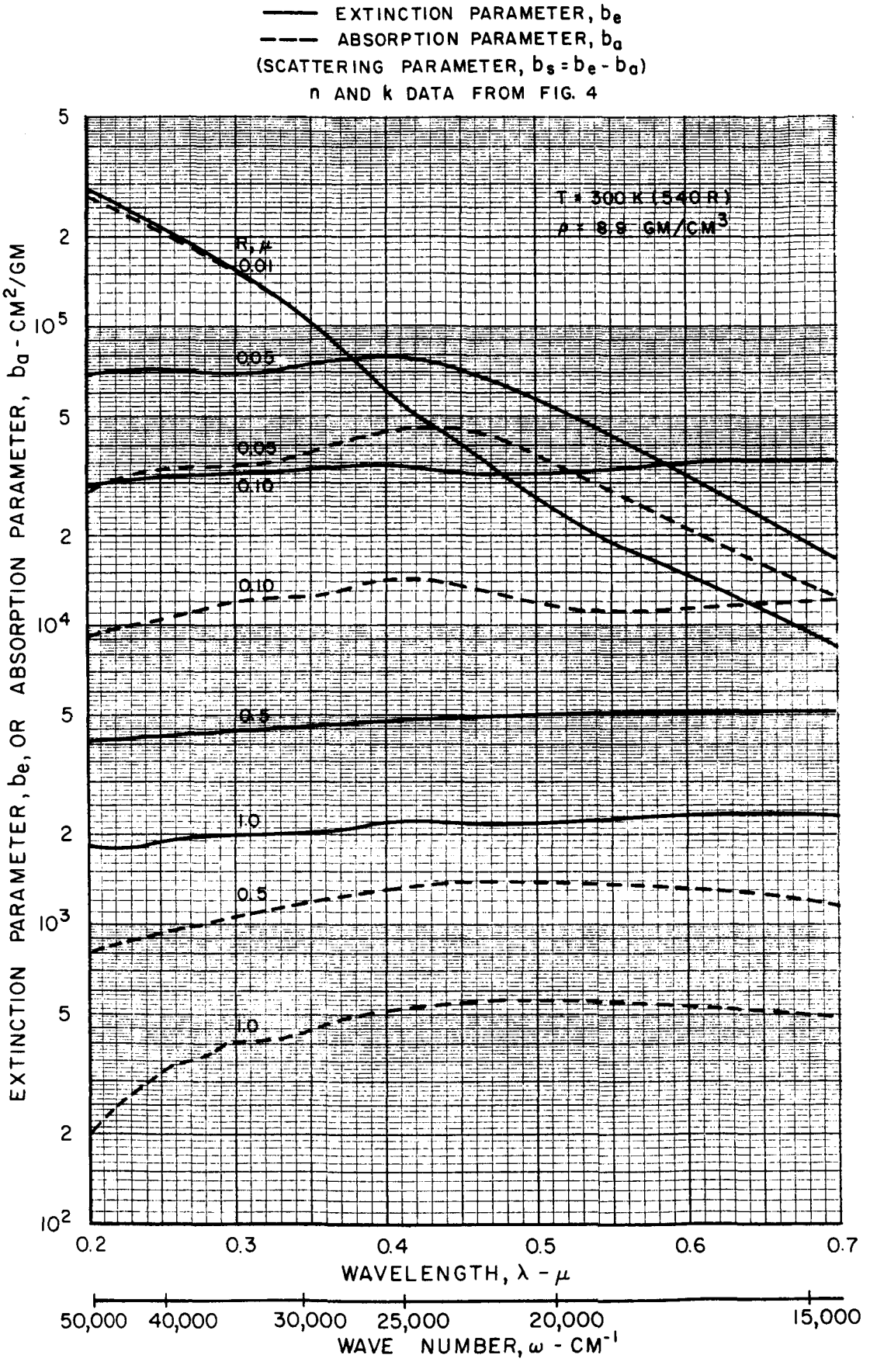

EFFECT OF WAVELENGTH ON THE EXTINCTION AND ABSORPTION PARAMETERS OF SPHERICAL TUNGSTEN PARTICLES

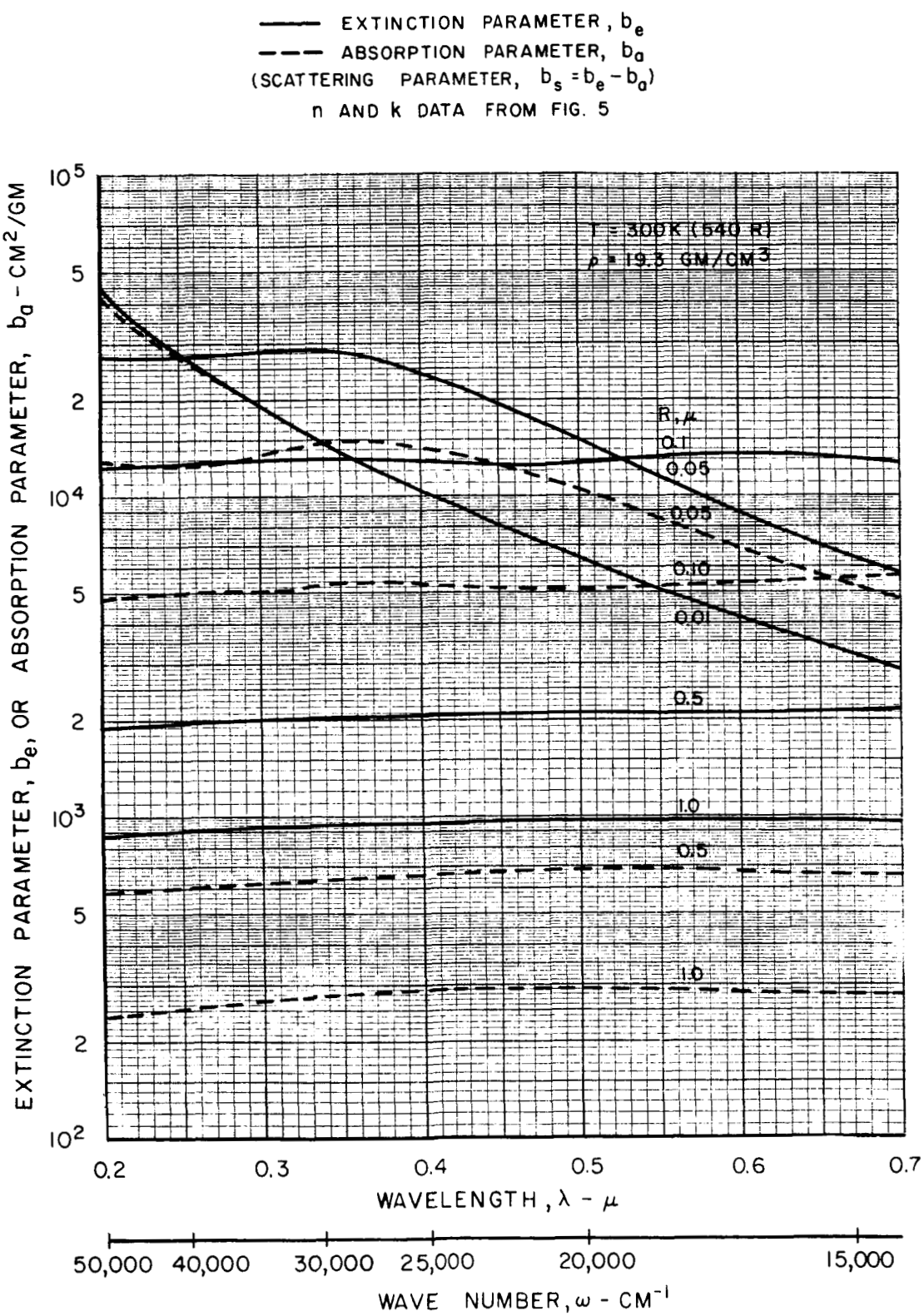

EFFECT OF WAVELENGTH ON THE ABSORPTION PARAMETER OF SPHERICAL MOLYBDENUM PARTICLES

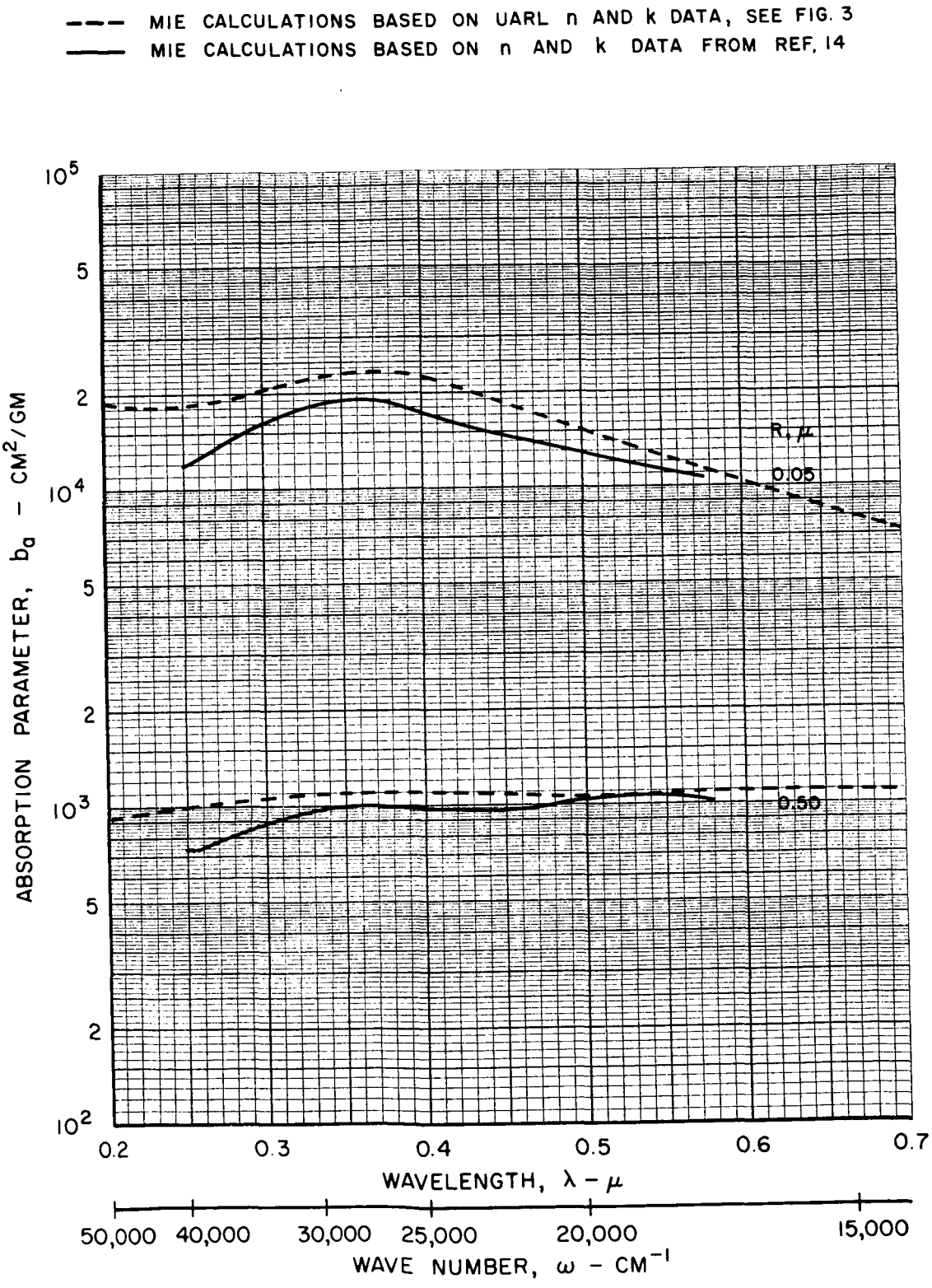

EFFECT OF WAVELENGTH ON THE ABSORPTION PARAMETER OF SPHERICAL TUNGSTEN PARTICLES

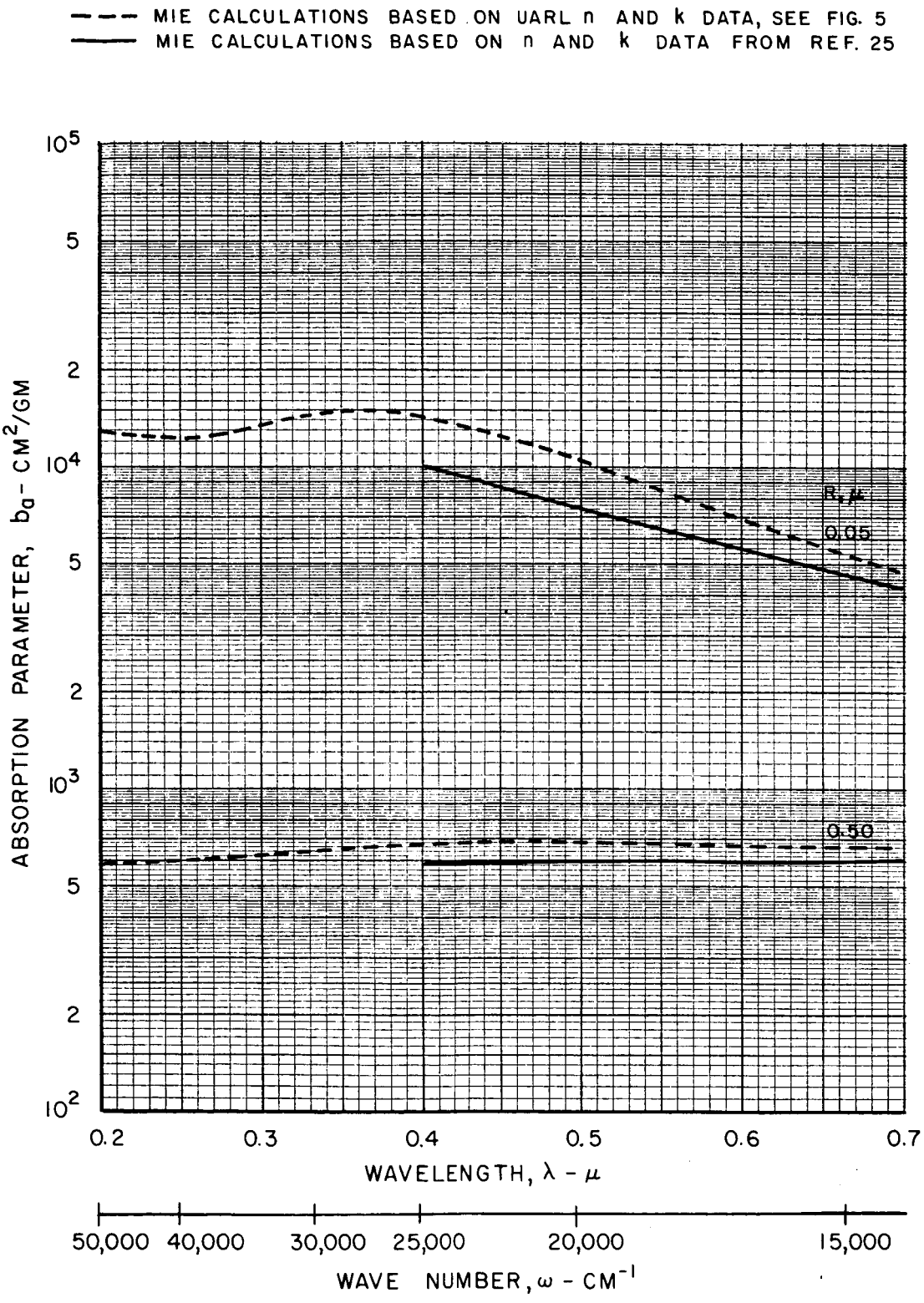

FIG. 22

COMPARISON OF THE ABSORPTION PARAMETERS OF MATERIALS INVESTIGATED FOR WAVELENGTHS BETWEEN 0.2 AND 1.0 MICRONS

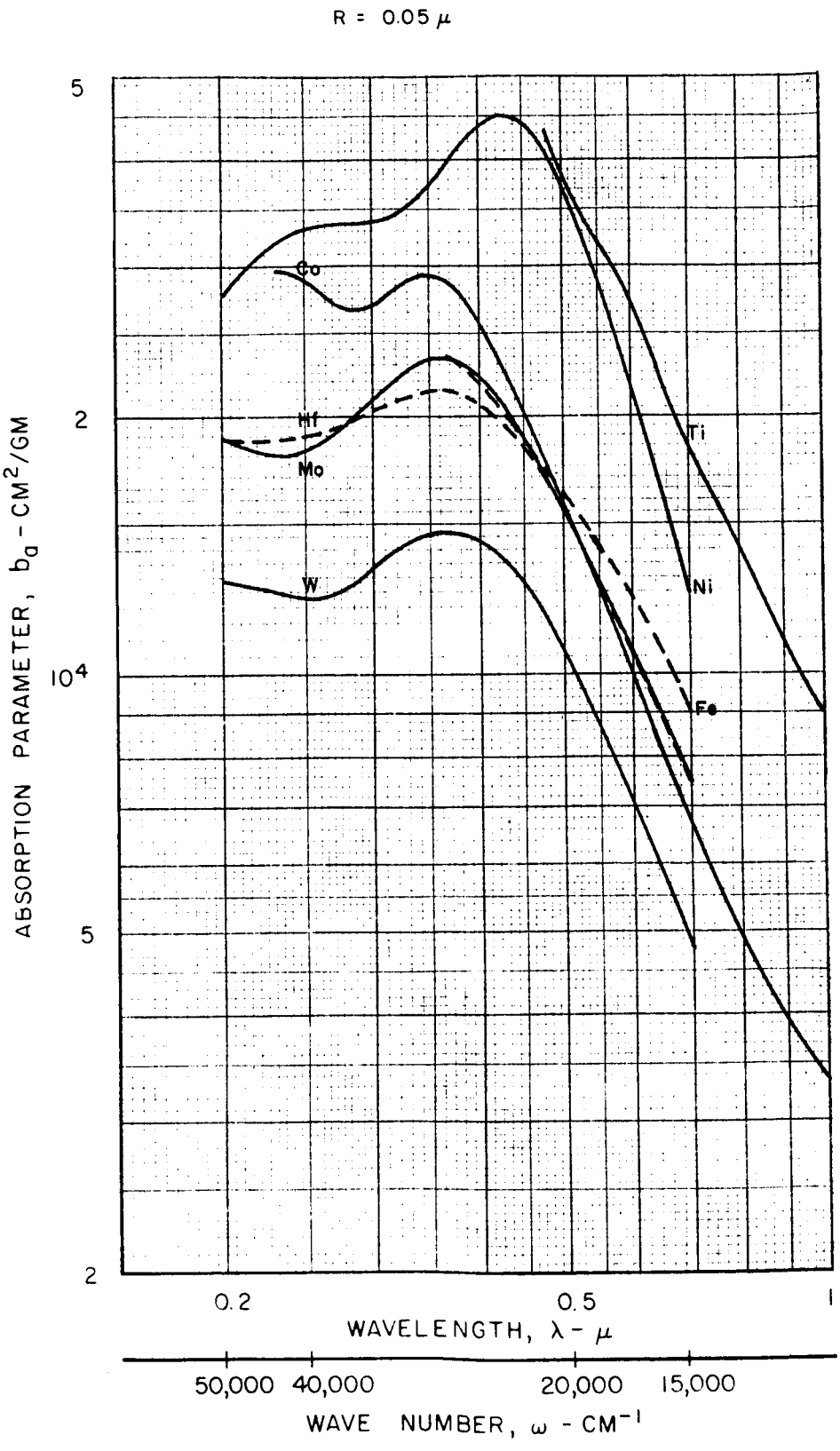

COMPARISON OF THE ABSORPTION PARAMETERS OF MATERIALS INVESTIGATED FOR WAVELENGTHS BETWEEN 1 AND 20 MICRONS

R = 0.05 μ

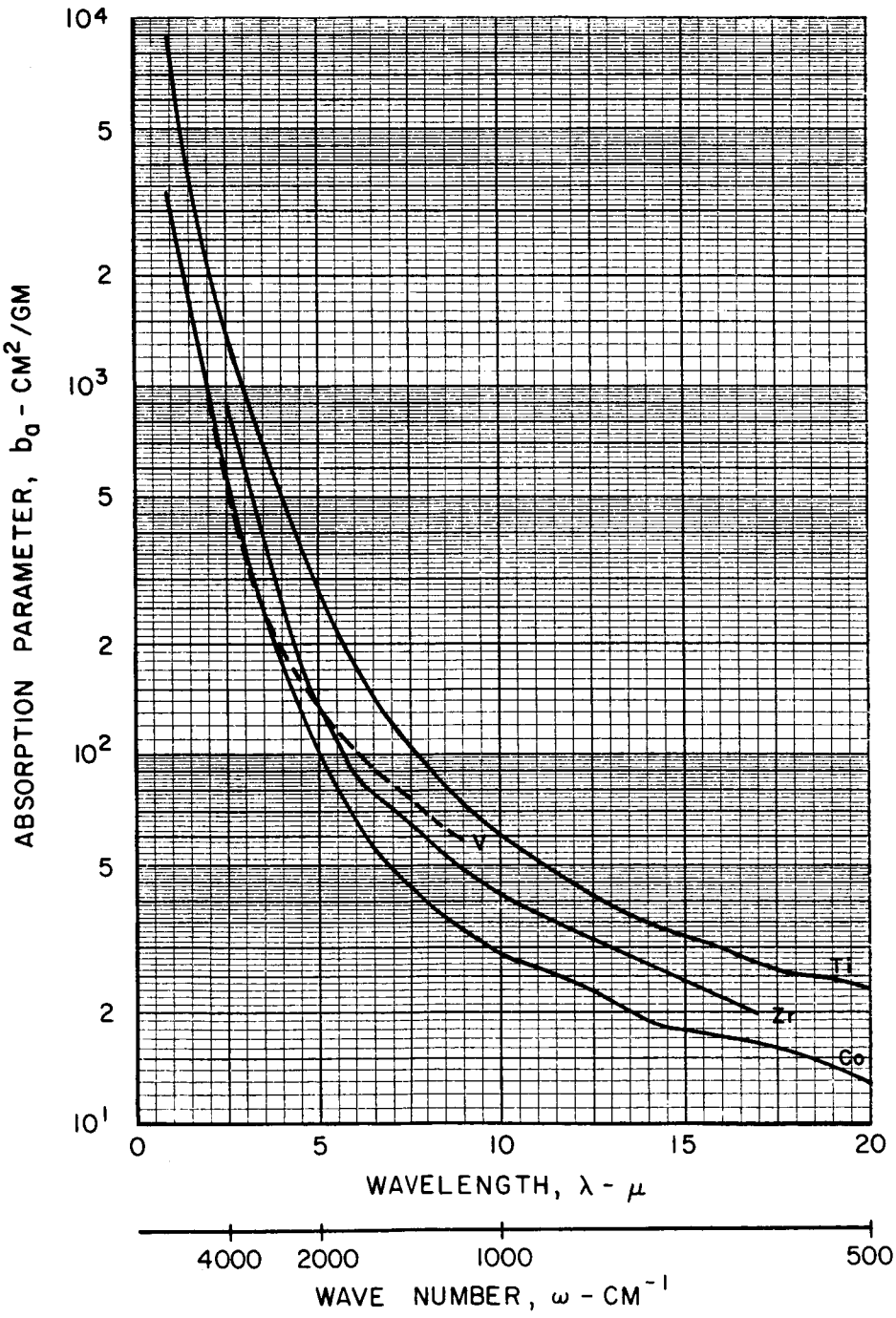

EFFECT OF WAVE NUMBER ON THE ABSORPTION PARAMETER OF SPHERICAL TUNGSTEN PARTICLES

R = 0.05 μ

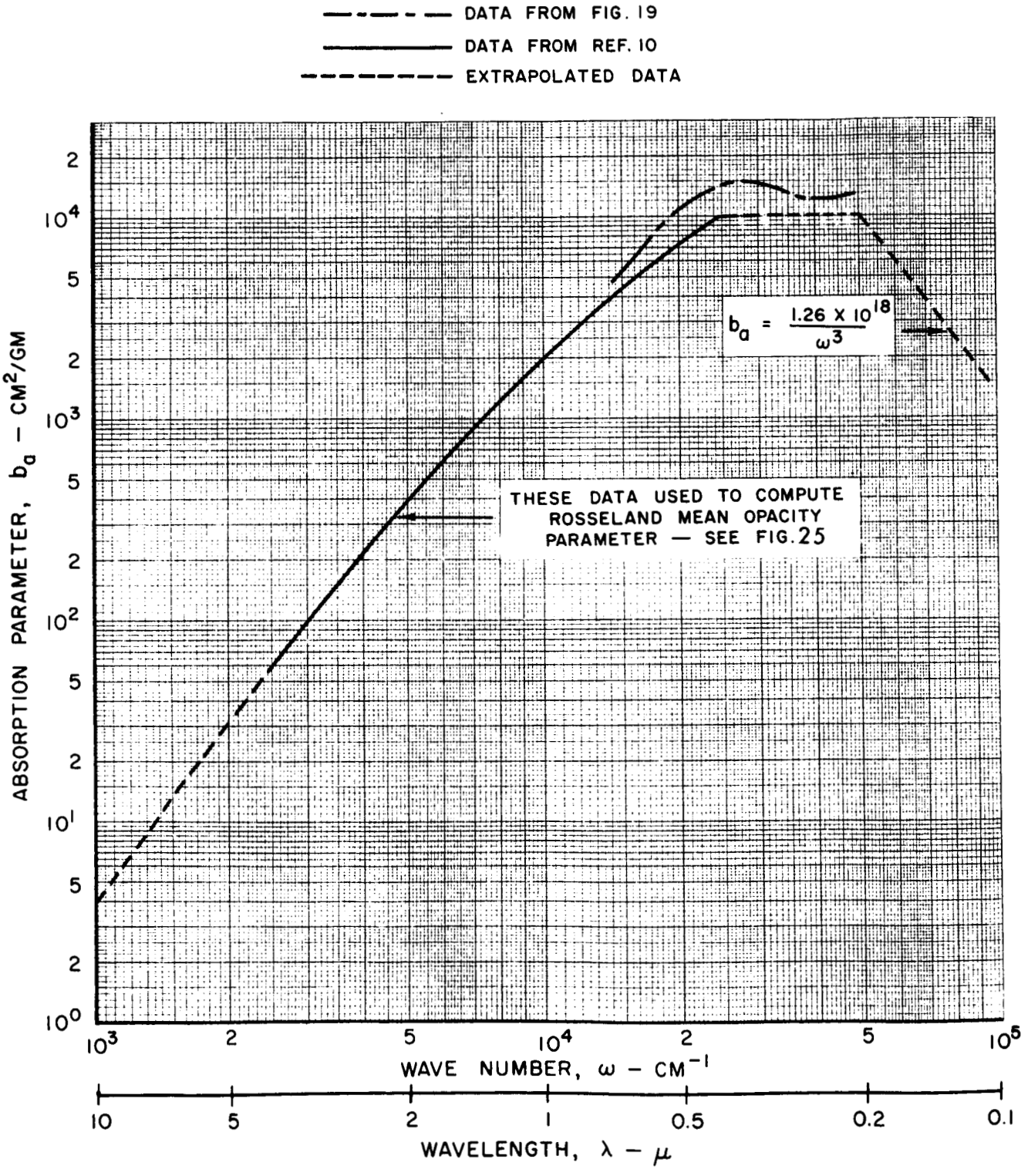

EFFECT OF TEMPERATURE ON THE ROSSELAND MEAN OPACITY PARAMETER OF SPHERICAL TUNGSTEN PARTICLES

$R = 0.05\,\mu$

SPECTRAL DATA FROM FIG. 24

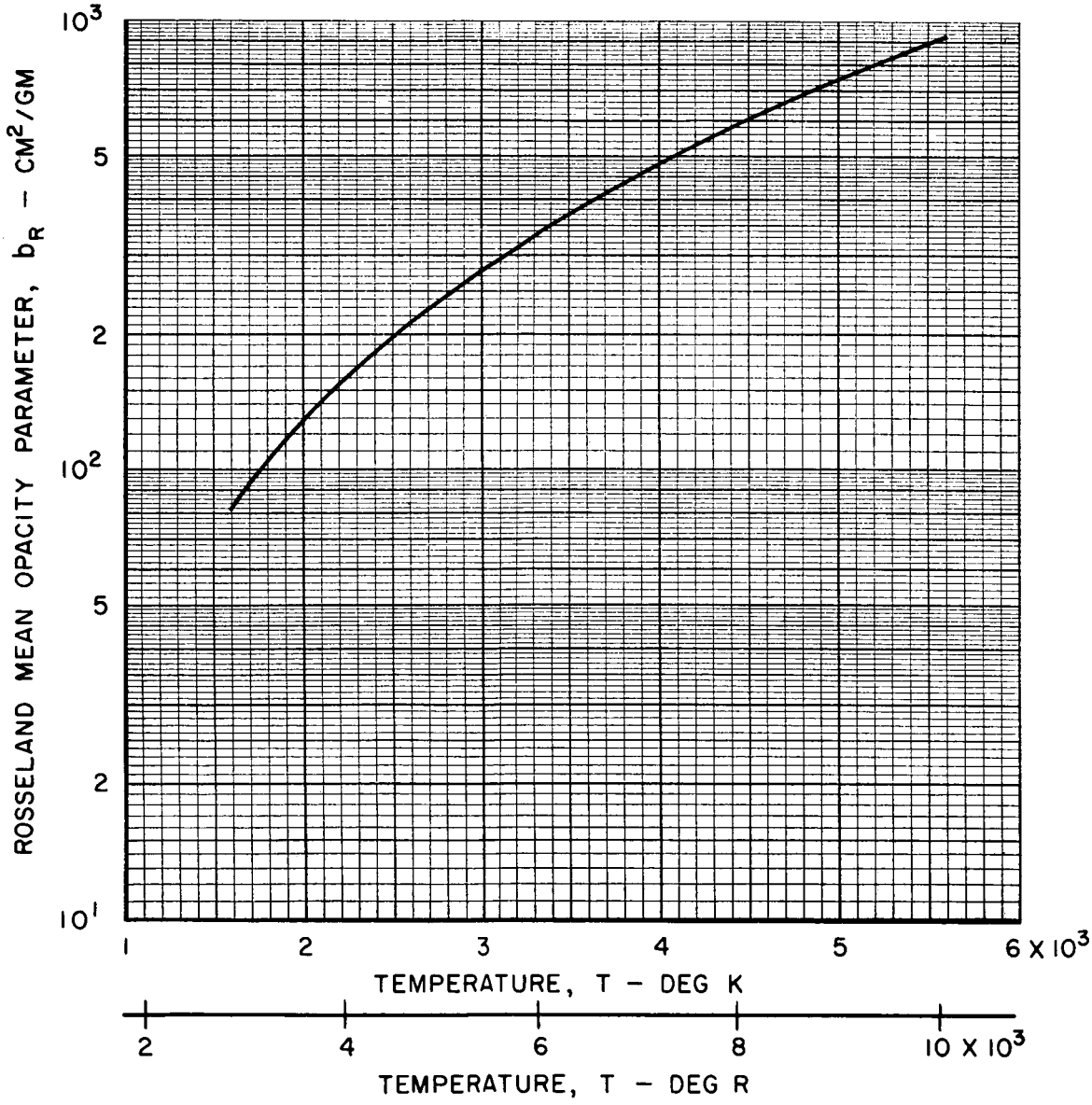

COMPUTED VARIATION OF THE REAL PART OF THE COMPLEX REFRACTIVE INDEX WITH ANALYZER SETTING FOR VARIOUS POLARIZER SETTINGS

ZERO SETTING LIES IN PLANE OF INCIDENCE WHICH INCLUDES NORMAL TO SAMPLE

COMPLEX REFRACTIVE INDEX $N = n - ik$

ANGLE OF INCIDENCE, ϕ - 65 DEG

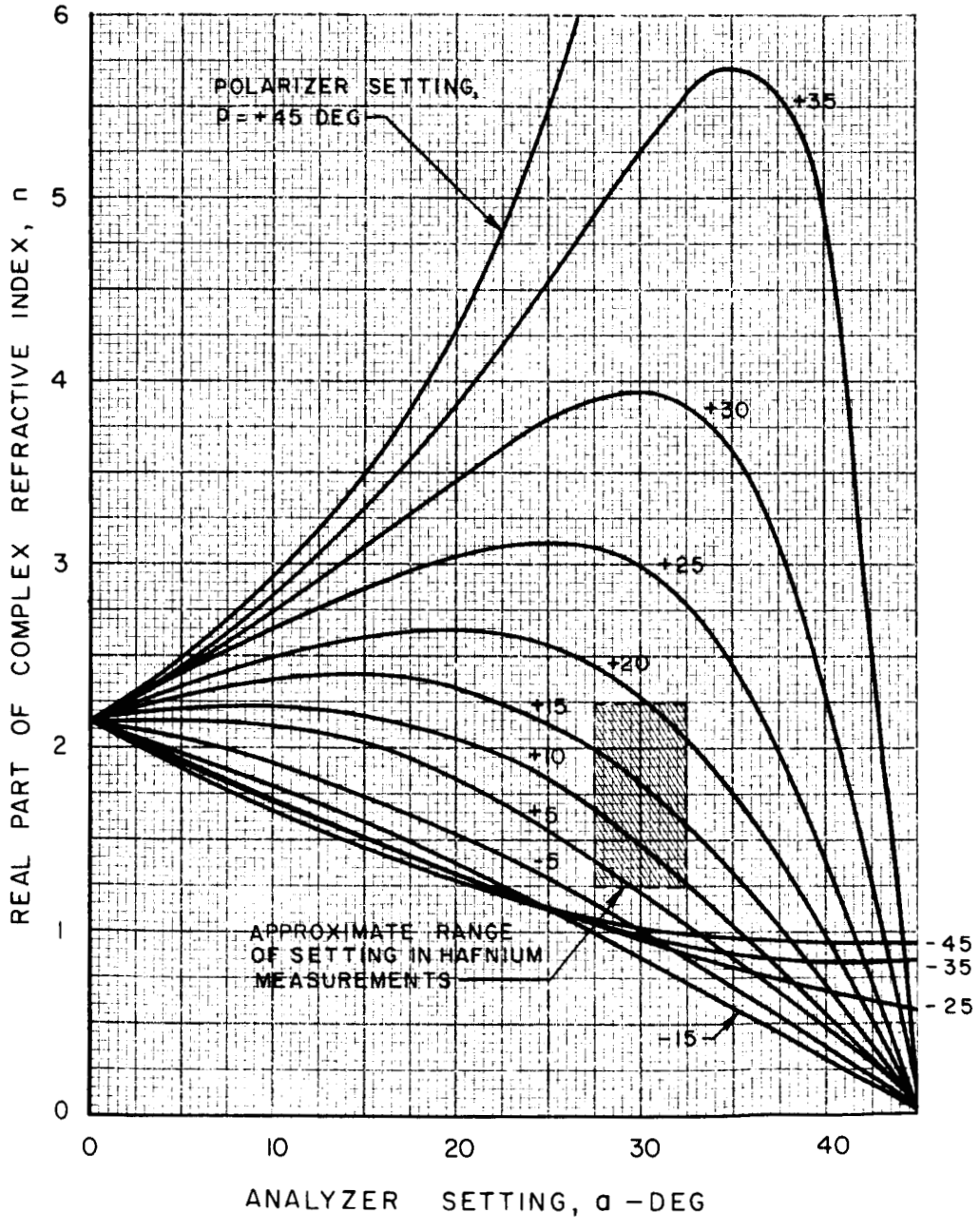

COMPUTED VARIATION OF THE IMAGINARY PART OF THE COMPLEX REFRACTIVE INDEX WITH ANALYZER SETTING FOR VARIOUS POLARIZER SETTINGS

ZERO SETTING LIES IN PLANE OF INCIDENCE WHICH INCLUDES NORMAL TO SAMPLE

COMPLEX REFRACTIVE INDEX $N = n - ik$

ANGLE OF INCIDENCE, ϕ - 65 DEG

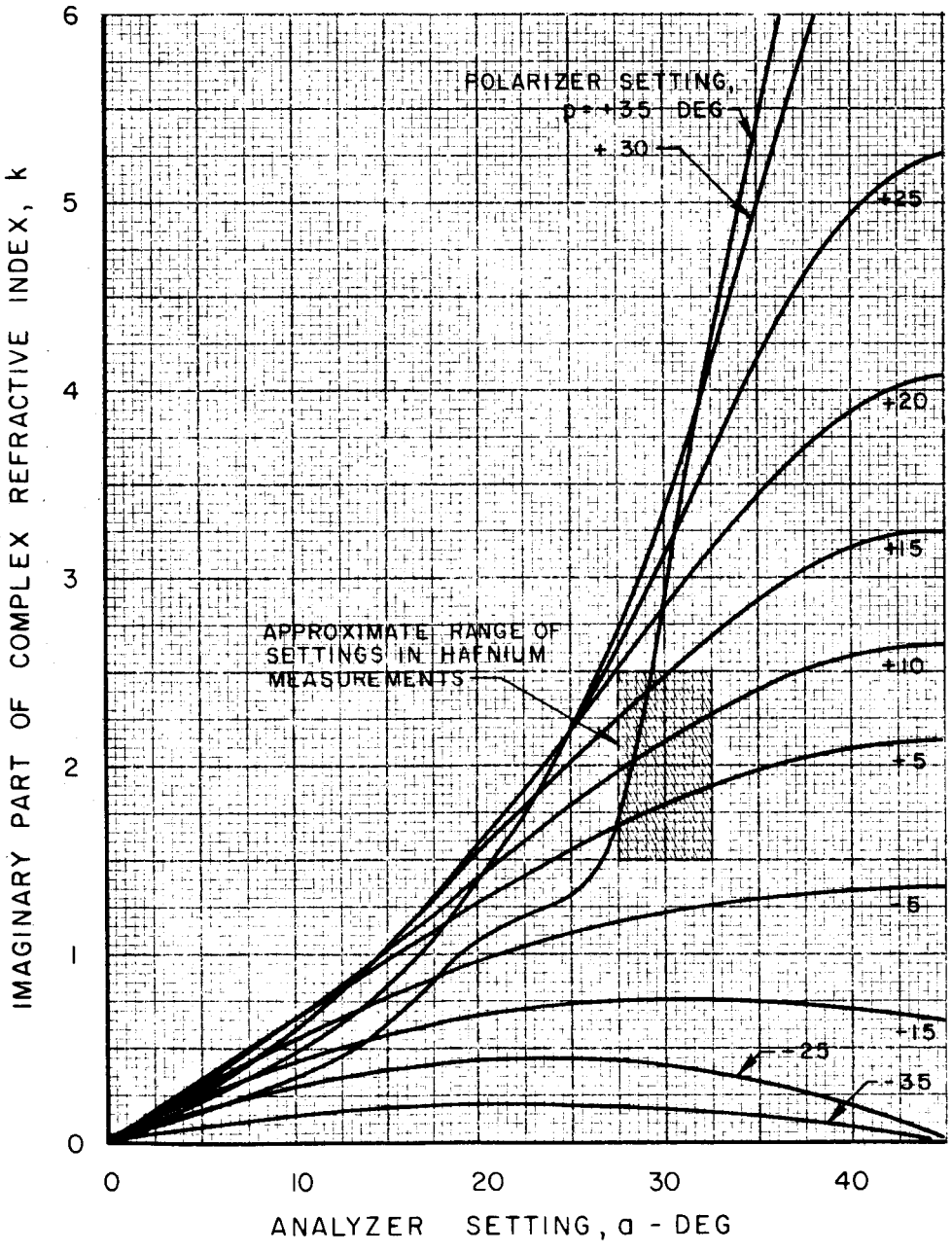

TYPICAL VARIATION OF POLARIZER AND ANALYZER SETTINGS WITH WAVELENGTH BETWEEN 0.2 μ AND 0.7 μ

MOLYBDENUM SAMPLE
COMPENSATOR FAST AXIS AT -45 DEG
COMPENSATOR RETARDATION 90 DEG

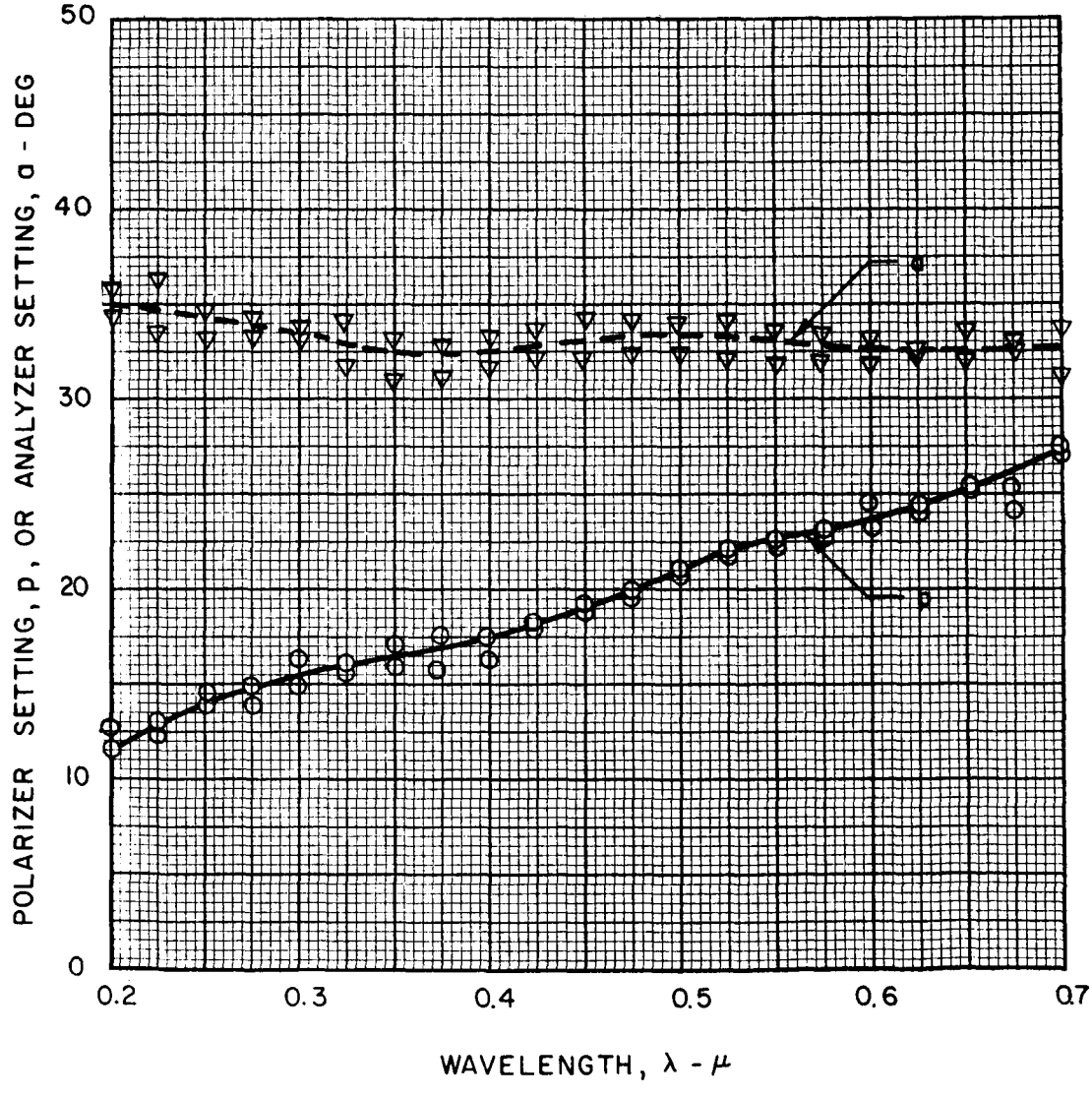

FIG. 29

EFFECT OF ANALYZER SETTING ON TRANSMITTED INTENSITY OF PLANE POLARIZED LIGHT REACHING DETECTOR AFTER REFLECTION FROM SAMPLE

ANALYZER AND POLARIZER SETTINGS ARE ROTATIONS RELATIVE TO PLANE OF INCIDENCE

MOLYBDENUM SAMPLE
WAVELENGTH, λ - 0.55 μ
POLARIZER SETTING, p - 20.10 DEG
COMPENSATOR FAST AXIS AT -45 DEG
COMPENSATOR RETARDATION 90 DEG

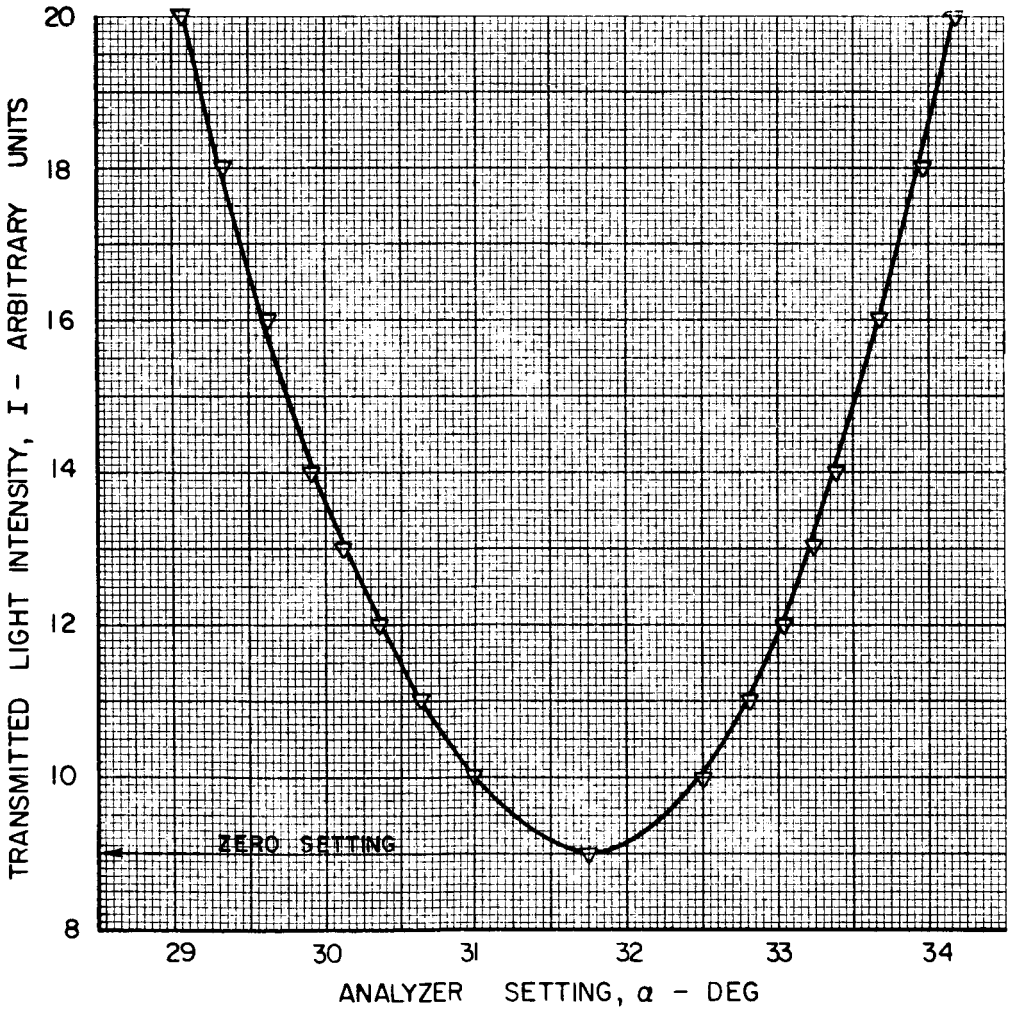

EFFECT OF POLARIZER SETTING ON TRANSMITTED INTENSITY OF PLANE POLARIZED LIGHT REACHING DETECTOR AFTER REFLECTION FROM SAMPLE

ANALYZER AND POLARIZER SETTINGS ARE ROTATIONS RELATIVE TO PLANE OF INCIDENCE

MOLYBDENUM SAMPLE
WAVELENGTH, λ – 0.55 μ
ANALYZER SETTING, α – 31.70 DEG
COMPENSATOR FAST AXIS AT -45 DEG
COMPENSATOR RETARDATION 90 DEG

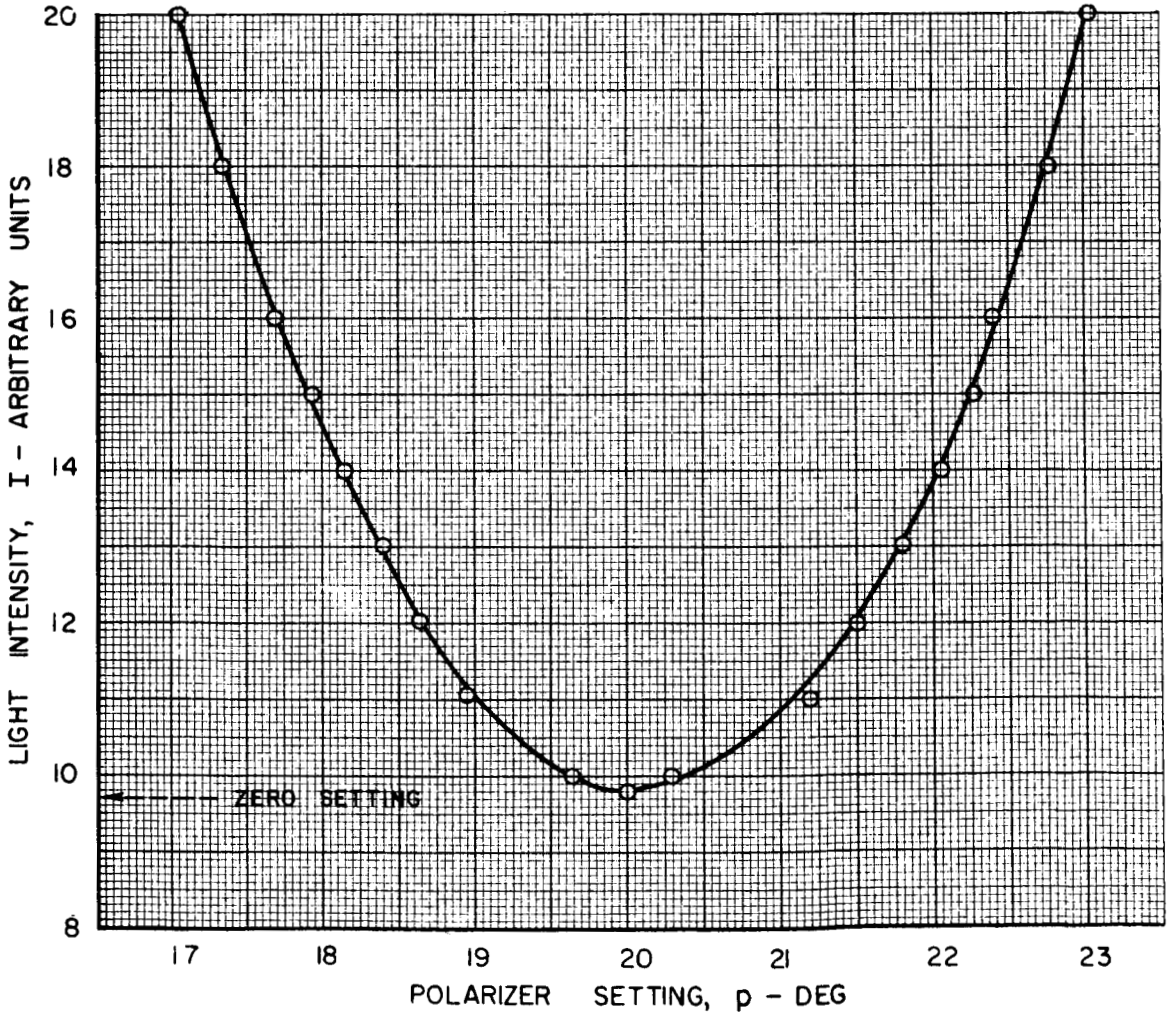

EFFECT OF COMPENSATOR RETARDATION ON REAL AND IMAGINARY PARTS OF COMPLEX REFRACTIVE INDEX OF MOLYBDENUM AT 0.55 μ

COMPLEX REFRACTIVE INDEX $N = n - ik$
COMPENSATOR FAST AXIS AT -45 DEG

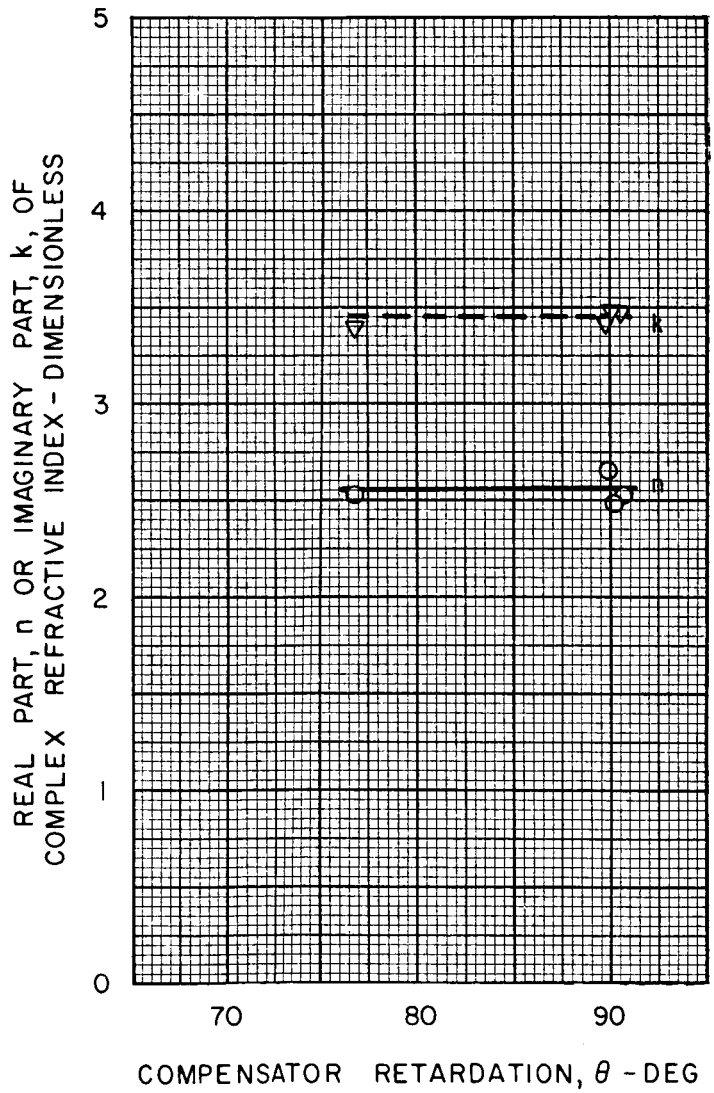

EFFECT OF ANGLE OF INCIDENCE ON THE MEASURED REAL AND IMAGINARY PARTS OF THE COMPLEX REFRACTIVE INDEX OF HAFNIUM, MOLYBDENUM AND TUNGSTEN AT A WAVELENGTH OF 0.55 μ
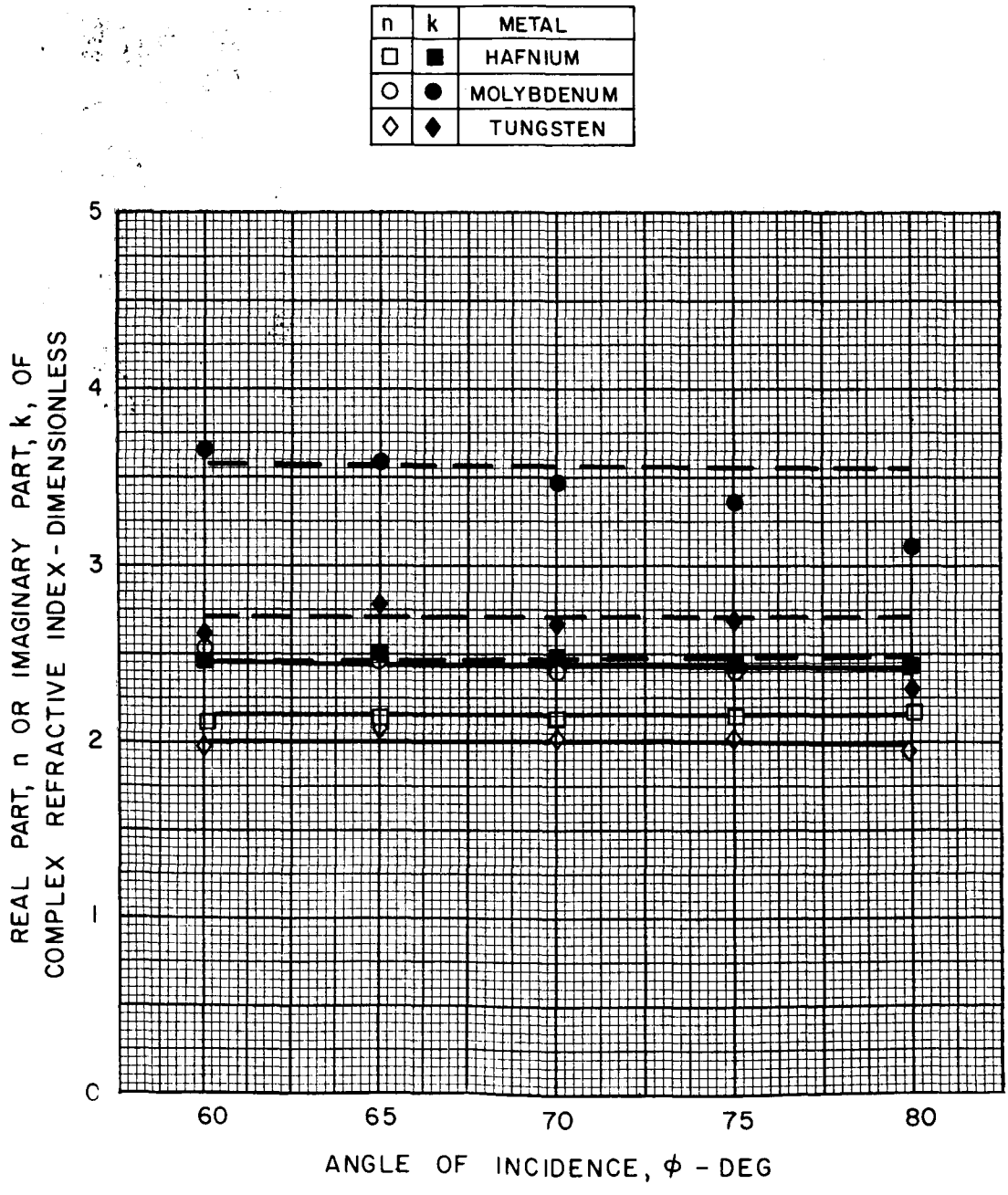
COMPLEX REFRACTIVE INDEX $N = n - ik$